



NTNU – Trondheim
Norwegian University of
Science and Technology

Wake behind a wind turbine operating in yaw

Birgitte Andresen

Master of Energy and Environmental Engineering
Submission date: June 2013
Supervisor: Per-Åge Krogstad, EPT

Norwegian University of Science and Technology
Department of Energy and Process Engineering

EPT-M-2013-9

MASTER THESIS
for
student Birgitte Andresen
Spring 2013
Wake behind a wind turbine operating in yaw
Wake bak en vindturbin som står skrått på vinden

Background and objective

In a wind park there is strong interaction between the turbines when the wind is directed along the direction of the turbine array. This effect has been mapped for turbines organized along a straight line where the wake from one turbine is fully emerged in the wake of the turbine upstream. Although this is the most simple case to study, it is not a very likely event. Due to the meandering of the wake and yawed operation of the upstream turbine, most of the time the downstream turbine is only exposed to part of the wake.

In order to study this effect in more detail, it is of interest to study the performance of two turbines mounted in-line, but where the downstream turbine is only partly affected by the wake of the upstream turbine. This may be simulated by yawing the upstream turbine, which produces a deflected and asymmetric wake.

The following tasks are to be considered:

- 1) The student should study how the wake is deflected and deformed as the yaw angle is increased. The performance effects on the characteristics of the turbine (C_T and C_P) should also be documented.
- 2) Once the characteristics of single turbine has been mapped, a second turbine should be mounted downstream of the first turbine and its performance characteristics should be mapped.

Within 14 days of receiving the written text on the master thesis, the candidate shall submit a research plan for his project to the department.

When the thesis is evaluated, emphasis is put on processing of the results, and that they are presented in tabular and/or graphic form in a clear manner, and that they are analyzed carefully.

The thesis should be formulated as a research report with summary both in English and Norwegian, conclusion, literature references, table of contents etc. During the preparation of the text, the candidate should make an effort to produce a well-structured and easily readable report. In order to ease the evaluation of the thesis, it is important that the cross-references are correct. In the making of the report, strong emphasis should be placed on both a thorough discussion of the results and an orderly presentation.

The candidate is requested to initiate and keep close contact with his/her academic supervisor(s) throughout the working period. The candidate must follow the rules and regulations of NTNU as well as passive directions given by the Department of Energy and Process Engineering.

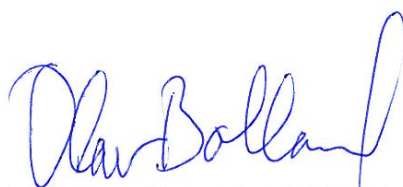
Risk assessment of the candidate's work shall be carried out according to the department's procedures. The risk assessment must be documented and included as part of the final report. Events related to the candidate's work adversely affecting the health, safety or security, must be documented and included as part of the final report. If the documentation on risk assessment represents a large number of pages, the full version is to be submitted electronically to the supervisor and an excerpt is included in the report.

Pursuant to "Regulations concerning the supplementary provisions to the technology study program/Master of Science" at NTNU §20, the Department reserves the permission to utilize all the results and data for teaching and research purposes as well as in future publications.

The final report is to be submitted digitally in DAIM. An executive summary of the thesis including title, student's name, supervisor's name, year, department name, and NTNU's logo and name, shall be submitted to the department as a separate pdf file. Based on an agreement with the supervisor, the final report and other material and documents may be given to the supervisor in digital format.

- Work to be done in lab (Water power lab, Fluids engineering lab, Thermal engineering lab)
 Field work

Department of Energy and Process Engineering, 14. January 2013



Olav Bolland
Department Head



Per-Åge Krogstad
Academic Supervisor

Preface

This master's thesis is submitted to the Norwegian University of Science and Technology (NTNU) as a conclusion of my Master of Science in Energy and Environmental Engineering. The five-year master degree of Energy and Environmental Engineering offers specialization after the 2nd and 3rd year, which has given me the opportunity of studying Heat and Energy Processes with specialization in Fluid Mechanics. Throughout the years spent at NTNU, including one year at the University of Hawaii at Mānoa as an exchange student, my interests have been particularly directed towards Renewable Energy. The present study has included tests in the wind tunnel at the Department of Energy and Process Engineering at NTNU, as well as calculations and numerical computations.

I wish to acknowledge my gratitude to my supervisor Per-Åge Krogstad for giving me the opportunity of working on this thesis, and also for guidance and advice throughout this whole process. I also want to thank Pål Egil Eriksen for assisting me through numerous hours in the wind tunnel laboratory and for helping me with the post-processing of the experimental data. Finally, a big thanks goes to Arnt Egil Kolstad for continuously helping me setting up the equipment in the laboratory.



Birgitte Andresen Trondheim, 10.06.2013

Abstract

The object of this study is primarily to understand the behavior of the wake behind a yawed turbine, and if yaw can be a method for actively controlling the direction of the wake, and thereby controlling the power output of downstream turbines.

Two model wind turbines were tested experimentally in the wind tunnel at NTNU. First of all, the performance of a single upstream turbine operating at fixed rotational speed with varying yaw angles was examined. Further, the aim was to understand to what extent the side force created by the yawed turbine affects the wake, thus the velocity deficits and turbulence intensities in the downstream flow field were experimented on. In addition, the performance and dynamic loads experienced by a second turbine operating at 3D downstream of the upstream turbine were examined. Finally, the overall efficiency of the wind farm was found for the different yaw scenarios.

The study confirms that when a turbine is operating in yaw, both the power and thrust coefficient will decrease significantly with increasing yaw angle. Yawing the upstream turbine will also affect the behavior of the wake to a great extent, as the wake is deformed and deflected sideways. When the upstream turbine is yawed 40° , the width of the wake at 3D downstream is decreased to half its size of un-yawed condition and is shifted about 0.5D sideways. The performance of the downstream turbine increases with increasing yaw angle of the upstream turbine. When the upstream turbine is yawed 50° , the downstream turbine obtains a power gain of 24% compared to the un-yawed condition, resulting in a maximum power coefficient of 33%. This confirms that the second turbine experiences less interaction with an upstream turbine operating under yawed conditions.

It was found that the optimal wind farm efficiency of the two model turbines occurs when the upstream turbine is yawed between 0° to 30° , resulting in a wind farm efficiency of approximately 54% for all three conditions. The power loss experienced by the upstream turbine is offset by the corresponding power gain of the downstream turbine. However, fatigue loads were found to act on both the turbine operating in yaw and the downstream turbine partly exposed to the wake, which will eventually reduce their longevity. Therefore, the result of the study carried out on two wind turbines in the wind tunnel suggests that it will not be beneficial to use yaw as a mechanism for controlling the wake direction and thereby increase the wind farm efficiency since the power gain of the downstream turbine will be offset by the power loss of the yawed turbine. Tailoring the blade design of the yawed turbines may, however, have a positive impact on the overall wind farm efficiency and also reduce fatigue loads.

Sammendrag

Formålet med dette studiet er hovedsakelig å forstå hvordan vaken bak en vindturbin som står skrått på vinden vil oppføre seg, og om å skråstille turbinen kan være en metode for å aktivt kontrollere retningen til vaken, og dermed forbedre ytelsen til turbiner plassert nedstrøms.

To vindturbinmodeller ble testet eksperimentelt i vindtunnelen på NTNU. Ytelsen til en enkelt turbin som opererte med konstant rotasjonshastighet med varierende innstrømningsvinkler ble undersøkt. Videre var målet å forstå hvilken grad sidekraften som oppstår fra den skråstilte turbinen påvirker vaken og strømningsutviklingen nedstrøms. Det ble derfor eksperimentert med endringer i hastighet og intensitet i nedstrøms turbulens. I tillegg ble ytelse og dynamisk last som virker på en turbin plassert 3D nedstrøms undersøkt. Total virkningsgrad for vindparken bestående av de to vindturbinmodellene med de forskjellige tilfellene for skjev innstrømning på oppstrømsturbinen ble til slutt sett på.

Studiet bekrefter at når en turbin står skrått på vinden vil virkningsgraden minke betraktelig med økende innstrømningsvinkel.

Når en turbin opplever skjev innstrømning vil dette i stor grad påvirke vaken i den forstand at den deformeres og bøyes av til siden. Når turbinen opererer med en innstrømningsvinkel på 40° vil bredden på vaken 3D nedstrøms reduseres til halvparten av opprinnelig bredde og forflyttes 0.5D til siden. Nedstrømsturbinen opplever en kontinuerlig økning i ytelse med økende innstrømningsvinkel på oppstrømsturbinen. For en innstrømningsvinkel på 50° vil nedstrømsturbinen ha en økt ytelse på 24%, noe som resulterer i en maksimal virkningsgrad på 33%. Dette bekrefter at ytelsen til nedstrømsturbinen vil bli mindre påvirket når oppstrømsturbinen står skrått på vinden.

Det ble funnet at optimal virkningsgrad av vindparken bestående av to vindturbinmodeller oppstår når oppstrømsturbinen har en innstrømsvinkel på 0° til 30° , som gir en virkningsgrad på 54 % for alle tre tilfeller. Effekttapet som oppstrømsturbinen opplever oppveies med tilsvarende økning i ytelse på nedstrømsturbinen. Når dette er sagt vil både turbinen som står skrått på vinden og turbinen som er delvis eksponert for vaken etter hvert oppleve redusert levetid, grunnet asymmetrisk last som sliter på turbinene. Konklusjonen på dette studiet utført på to vindturbiner i vindtunnel er følgelig at det ikke vil være lønnsomt å skråstille turbinen for å kontrollere retningen til vaken og dermed få økt virkningsgrad på vindparken, siden effektøkningen i nedstrømsturbinen vil oppveies av effekttapet til turbinen med skjev innstrømning. Skreddersydd design av bladene til den skråstilte turbinen kan derimot muligens ha en positiv innvirkning på vindparkens virkningsgrad og også redusere slitasje.

Contents

1	Introduction	1
2	Aerodynamics of wind turbines.....	3
2.1	The potential of wind energy	3
2.2	Theoretical estimate of power production	3
2.2.1	Betz limit	6
2.3	Wind turbines: principles and design.....	7
2.3.1	Power control.....	7
2.3.2	Tip speed ratio	9
3	Wind and wakes	11
3.1	Wind turbine wakes and turbulence.....	11
3.1.1	Turbulence intensity	12
3.2	Wake interference in wind farms.....	14
3.3	Effect of yaw	16
3.3.1	Momentum theory for a wind turbine operating in yaw	17
3.3.2	Wake control and yawing	19
4	Experimental set-up and methods.....	21
4.1	Wind tunnel and model turbines.....	21
4.2	Scaling and blockage effects.....	24
4.3	Measurement techniques.....	24
4.3.1	Pitot-static tube.....	25
4.3.2	Hot-wire anemometer	26
4.4	Calibration.....	31
4.4.1	Torque	31
4.4.2	Thrust	32
4.4.3	Pressure transducers.....	32
4.4.4	Hot-wire anemometer	33
4.5	Measurement inaccuracies.....	34
5	Procedure.....	35
5.1	Single model turbine operating in yaw	36
5.1.1	Performance	36
5.1.2	Downstream flow field	36
5.2	Wake interference on a second (downstream) model turbine	38
5.2.1	Performance	38
5.2.2	Dynamic loads.....	38
5.3	Free stream velocity.....	39
6	Results and discussion.....	41
6.1	Single model turbine operating in yaw	41
6.1.1	Performance	41
6.1.2	Downstream flow field	44
6.2	Wake interference on a second (downstream) model turbine	52
6.2.1	Performance	52
6.2.2	Dynamic loads	54
6.3	Wind farm efficiency	56
7	Conclusion.....	58
8	Further work.....	60
9	Bibliography.....	61
APPENDIX A	Calibration	I
A. 1	Torque	I
A. 2	Thrust	III
A. 3	Pressure transducers	IV

A. 3. 1	Pitot-static tube.....	IV
A. 3. 2	Contraction	V
A. 4	Hot-wire anemometer.....	VI
APPENDIX B		VII

List of Figures

Figure 2.1 – Actuator disk model of a wind turbine [1]	4
Figure 2.2 – Cross section of a rotor blade with the angle of attack, α	7
Figure 2.3 – Cross section of a rotor blade with pitching moment [1]	8
Figure 2.4 – Power curve of a pitch and stall-regulated wind turbine [6]	9
Figure 2.5 – Theoretical maximum power coefficient as a function of tip speed ratio for an ideal wind turbine, with and without wake rotation. [1]	10
Figure 3.1 – Velocity profile in the wake of a turbine [8].....	12
Figure 3.2 – Wake behind wind turbines in an array[13]	14
Figure 3.3 – Yawed turbine with yaw angle, γ . [16].....	16
Figure 3.4 – Yawed inflow with skewed wake and induced velocities. [18].....	17
Figure 3.5 – The deflected vortex wake of a yawed turbine, with skew angle χ . [18]	19
Figure 4.1 – The two wind turbine models in the wind tunnel	21
Figure 4.2 – The wind tunnel test section seen from above.....	22
Figure 4.3 – Pitot-static tube. [23].....	25
Figure 4.4 – Hot-wire probe. [27].....	26
Figure 4.5 – Constant temperature control circuit [25]	27
Figure 4.6 – Horizontal mean velocity profile of the pipe's cross-section.....	30
Figure 4.7 - Horizontal turbulent velocity profile of the pipe's cross-section, in the average flow direction.....	30
Figure 5.1 – Turbine B heavily disturbed by an un-yawed turbine A. By yawing turbine C, turbine D experience much less interaction with the wake produced.....	35
Figure 6.1 – Performance of the model turbine operating at zero yaw conditions	41
Figure 6.2 – Power coefficient for the model turbine at $\lambda = 6$ while varying yaw angles, γ	43
Figure 6.3 – Thrust coefficient for the model turbine at $\lambda = 6$ while varying yaw angles, γ	43
Figure 6.4 – Horizontal velocity profile with zero yaw	45
Figure 6.5 – Horizontal velocity profile with $\gamma = 20^\circ$	45
Figure 6.6 – Horizontal velocity profile with $\gamma = 40^\circ$	45
Figure 6.7 – Horizontal turbulence intensity profile at $x/D = 3$ downstream of the upstream turbine at zero yaw	49
Figure 6.8 – Horizontal turbulence intensity profile at $x/D = 3$ downstream of the upstream turbine yawed 20°	49
Figure 6.9 – Horizontal turbulence intensity profile at $x/D = 3$ downstream of the upstream turbine yawed 40°	49
Figure 6.10 – The performance of the second (downstream) turbine at $x/D = 3$ when the first (upstream) turbine operating at different yaw angles at design condition	52
Figure 6.11 – The maximum power coefficient of the second (downstream) turbine at $x/D = 3$ with the first (upstream) turbine operating at different yaw angles.....	53
Figure 6.12 – Mean torque experienced by the downstream turbine operating at different tip speed ratios, while the upstream turbine is operating in various yawed conditions.....	54
Figure 6.13 – Standard deviation of the torque experienced by the downstream turbine operating at different tip speed ratios, while the upstream turbine is operating in various yawed conditions	55
Figure 6.14 – Wind farm efficiency of the two turbines, where the downstream turbine is operating at maximum power coefficient at $x/D = 3$ when the upstream turbine is operating at varying yaw angles.....	56

Figure A. 1 – Calibration curve, torque.....	I
Figure A. 2 – Calibration curve, thrust.....	III
Figure A. 3 – Calibration curve, pitot-static tube.	IV
Figure A. 4 – Calibration curve, contraction.....	V
Figure A. 5 – Calibration curve, hot-wire anemometer.....	VI

List of tables

Table A. 1 – Calibration data, torque.....	II
Table A. 2 – Calibration data, thrust.	III
Table A. 3 – Calibration data, pitot-static tube.....	IV
Table A. 4 – Calibration data, contraction.....	V
Table A. 5 – Calibration data, hot-wire anemometer.....	VI

Nomenclature

Latin symbols

Symbol	Definition
A	Rotor area [m^2]
a	Axial induction factor [-]
C_p	Power coefficient [-]
C_T	Thrust coefficient [-]
D	Wind turbine diameter [m]
E	Voltage measurement [V]
F_T	Total shaft torque or moment [Nm]
g	Gravity [m/s^2]
h	Convective heat transfer coefficient [$\text{W/m}^2\text{K}$]
I	Current [A]
m	Mass [kg]
\dot{m}	Mass flow rate [kg/s]
P	Total wind turbine power [W]
Q	Volumetric flow rate [m^3/s] or heat flow [W]
R	Ideal gas constant [-]
$R_{\text{wire, c}}$	Wire resistance [Ω]
$R_{\text{wire, h}}$	Heated wire resistance [Ω]
R_{cable}	Cable resistance [Ω]
r	Wind turbine radius [m]
p	Pressure [Pa]
P	Power produced by a wind turbine [W]
T	Total wind turbine thrust force [N]
T	Temperature [K]
U	Free stream velocity [m/s]
U_x	Velocity at distance X downstream [m/s]
U_{ref}	Reference velocity and free stream velocity [m/s]
U^*	Friction velocity [m/s]
W	Power generated by heating [W]
x	Distance downstream of turbine [m]

Greek Symbols

Symbol	Definition
α	Angle of attack [°]
α	Temperature coefficient of wire material [K ⁻¹]
β	Overheating factor [-]
γ	Yaw angle [°]
η	Wind farm efficiency [-]
λ	Tip speed ratio [rad]
ρ	Density [kg/m ³]
σ	Standard deviation [-]
χ	Skew angle [°]
ω	Rotor rotational speed [rad/s]

1 Introduction

During the last couple of decades there has been an increased attention towards wind energy. Due to climate change, increasing demands and shortage of fossil fuels, renewable energy sources are more popular than ever. To make wind power competitive with other traditional energy sources it is important to minimize the cost per unit energy, thus maximize the power production.

To maximize the power output of a single wind turbine, the rotor should face in the direction of the wind inflow. However, most wind turbines operate tightly clustered in arrays, as economic constraints make it impossible to locate the turbines adequately apart to prevent them from interacting with each other. For certain wind directions, upstream turbines will affect the operating conditions of each individual turbine downstream in an array. This is referred to as the wake effect and is of great importance when designing effective wind farms. The most obvious effects of wake interaction in arrays are the velocity deficit and the increased turbulence causing higher loads on turbines downstream in an array. This naturally causes a reduction in the power output for downstream turbines. Therefore, it is advantageous to minimize the interaction between the wake from an upstream turbine and a downstream turbine. Yawing the upstream turbine may be a method for actively controlling the direction of the wake, thereby controlling the power output of downstream turbines and decreasing loads. One possibility is therefore to selectively yaw upstream turbines in such a way that their wakes are deflected away from neighboring turbines to obtain a better efficiency on the downstream turbines and also overall efficiency.

In this report, the following tasks are to be considered:

- The wake behind a yawed turbine is studied in terms of how the wake is deflected and deformed as the yaw angles increase. The mean velocity and the turbulence intensity are quantities looked at in the wake profile. The effect this has on the turbine's performance is also examined.
- The efficiency of a second turbine operating downstream of the yawed turbine is studied, where the downstream turbine is only exposed to part of the wake depending on the yaw angle of the upstream turbine. In addition, the dynamic loads experienced by the blades of the second turbine are examined with varying yaw angles of the upstream turbine.

- The overall efficiency of the two model turbines is studied.

Necessary understanding of physics of a wind turbine and airflow needed is presented in the sections 2 and 3.

2 Aerodynamics of wind turbines

Theory is introduced to get a better understanding of the aerodynamics of wind turbines.

2.1 The potential of wind energy

The energy potential in the wind lies within the kinetic energy. The full potential of the wind of a cross section is given by

$$\frac{P}{A} = \frac{1}{2} \rho U^3 \quad (2.1)$$

In practice, the real potential of the power generation from the wind for horizontal axis wind turbines is maximum 45% of this. [1] A wind turbine is not able to capture all of the wind's kinetic energy potential. If this was to happen, the air speed behind the turbine would be zero and new airflow would be blocked, not getting through the turbine. What happens when the wind approaches the turbine is described in the next section along with loss factors leading to a decrease in the real potential compared to the theoretical potential.

2.2 Theoretical estimate of power production

Betz law is derived from the principles of conservation of mass and momentum on the air stream flowing through an idealized "actuator disk" that extracts energy from the wind stream. It can be explained as a physical law showing that when the wind pushes the rotor to a wind turbine, the wind speed reduces, and the speed on the other side of the turbine will be lower than the speed before the turbine. The more energy that is captured from the wind, the lower speed will occur on the other side of the turbine. Betz law basically shows that if the wind speed is the same before and after the turbine, it is not possible to capture any energy from the wind.

Using a simple model based on linear momentum theory, the power from an ideal turbine rotor can be determined. This simple model is often referred to as 'Betz limit'. Besides from finding the power from an ideal turbine, it also determines the thrust of the wind on the ideal rotor and the effect of the rotor operation on the local wind field. Given that it is a simple model, certain assumptions for the turbine and the airflow must be made. Thus, the model is

only valid for an ideal turbine operating in a homogenous, incompressible, steady state fluid flow with no frictional drag.

A control volume shown in Figure 2.1 is used for setting up the power law around the turbine area. From conservation of mass and knowing that $U_1 > U_4$, it is known that also $A_4 > A_1$.

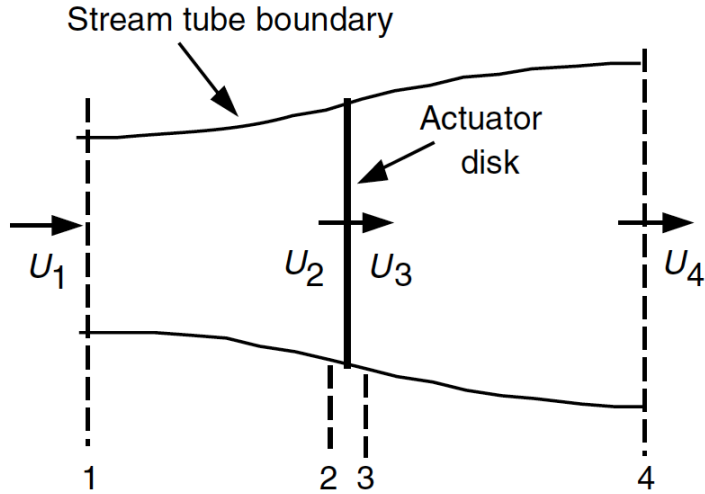


Figure 2.1 – Actuator disk model of a wind turbine [1]

Enclosing the whole system, the net forces on the control volume can be found. The net forces are equal and opposite to the thrust, T , which is the force from the wind acting on the wind turbine.

Betz limit can be derived starting with the conservation of linear momentum applied to the control volume, given by

$$T = U_1(\rho AU)_1 - U_4(\rho AU)_4 \quad (2.2)$$

From mass conservation and steady state flow assumptions, the mass flow rate is the same before and after the turbine, thus

$$(\rho AU)_1 = (\rho AU)_4 = \dot{m} \quad (2.3)$$

$$T = \dot{m}(U_1 - U_4) \quad (2.4)$$

Bernoulli's equation applied on both sides of the actuator disk is given by

$$p_1 + \frac{1}{2}\rho U_1^2 = p_2 + \frac{1}{2}\rho U_2^2 \quad \text{upstream} \quad (2.5)$$

$$p_3 + \frac{1}{2}\rho U_3^2 = p_4 + \frac{1}{2}\rho U_4^2 \quad \text{downstream} \quad (2.6)$$

From the assumptions of static pressure far upstream and static pressure far downstream of the rotor being equal, the thrust can also be expressed as the sum of forces on each side of the rotor

$$T = A_2(p_2 - p_3) \quad (2.7)$$

Substituting for p_2 and p_3 from Eq. (2.5) and (2.6), then

$$T = \frac{1}{2} \rho A_2 (U_1^2 - U_4^2) \quad (2.8)$$

Equating the thrust values from (2.2) and (2.4), and also making use of the mass flow rate from (2.3) an expression of the velocity at the rotor is obtained:

$$U_2 = \frac{U_1 + U_4}{2} \quad (2.9)$$

The expression above confirms that the rotor velocity is the average of the upstream and downstream velocity.

An axial induction factor is defined as:

$$a = \frac{U_1 - U_2}{U_1} \quad (2.10)$$

The axial induction factor is a measure of the velocity reduction between the free stream velocity and the rotor velocity. The velocity across the disk, the downstream velocity and the power of the turbine can be expressed, respectively, as

$$U_2 = U_1(1 - a) \quad (2.11)$$

$$U_4 = U_1(1 - 2a) \quad (2.12)$$

$$P = \frac{1}{2} \rho A U^3 4a(1 - a)^2 \quad (2.13)$$

where A is the cross-sectional area at the rotor and U is the free stream velocity.

The performance of the wind turbine is represented by the fraction of the power available in the wind and the extracted rotor power, and is characterized by the power coefficient, C_p :

$$C_p = \frac{P}{\frac{1}{2} \rho U^3 A} = 4a(1 - a)^2 \quad (2.14)$$

The axial thrust on the disk is obtained by combining equation (2.8) and (2.12)

$$T = \frac{1}{2} \rho A U^2 4a(1-a) \quad (2.15)$$

Similarly to the power, the thrust on a wind turbine is represented by the thrust coefficient, C_T :

$$C_T = \frac{T}{\frac{1}{2} \rho U^2 A} \quad (2.16)$$

The thrust coefficient, C_T , of an ideal wind turbine can also be expressed as $4a(1-a)$. The ideal wind turbine has its maximum of 1.0, when $a = 0.5$ and the downstream velocity equals zero. As this is an idealized model neglecting the complicated flow patterns that may occur in practice, the model is not valid for axial induction factors that exceed 0.5. Axial induction factors exceeding 0.5 will cause the thrust coefficient to exceed 1.0, and can result in a C_T as high as 2.0. [1] This will be further discussed later in the report.

2.2.1 Betz limit

Betz limit is the maximum theoretically possible rotor power coefficient, and presents how much an ideal turbine can capture of the kinetic energy in the wind. [2] Betz limit is obtained by taking the derivative of the power coefficient with respect to a , and setting it to zero. This results in $a = 1/3$ and a maximum theoretical power coefficient of $C_{p,\max} = 16/27$. The maximum power possible to extract from the wind is therefore approximately 59%. This is a very optimistic number, as this yield for the theoretical case. There are three effects leading to a decrease in the possible power output. These factors are the rotation of the wake behind the rotor, finite numbers of blades and related tip losses, and the fact that the aerodynamic drag is non-zero. In practice, 45 % is the maximum efficiency of a wind turbine.

2.3 Wind turbines: principles and design

When air is flowing around a streamlined body such as a wing profile, a pressure difference between the lower and upper side of the blade occur due to their shape and a force is therefore generated. The curvy side of the blade generates low air pressure, while the other side of the blade generates high air pressure. The force perpendicular to the flow direction is called lift, and the force parallel to the flow is called drag. The angle between the blades and the direction of the relative wind is called the angle of attack, as seen in Figure 2.2 below. As the blade itself is moving, the angle of attack is not just dependent on the wind direction. [3]

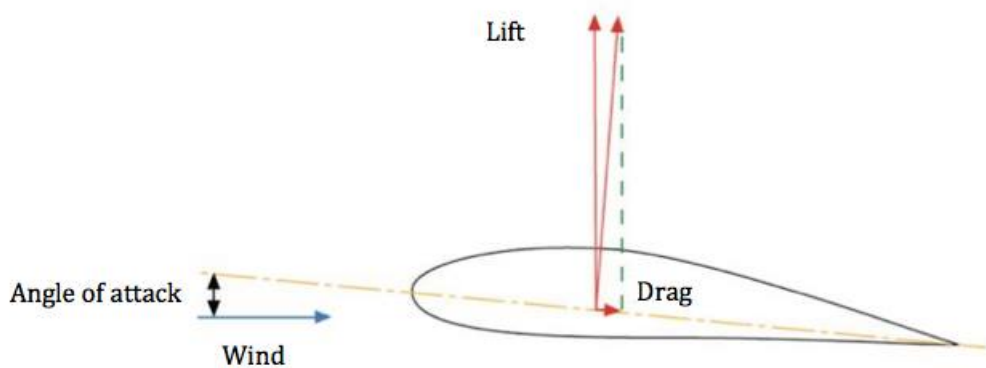


Figure 2.2 – Cross section of a rotor blade with the angle of attack, α .

2.3.1 Power control

As it is desirable to make the cost per produced energy unit competitive with other energy sources, the potential in the wind needs to be exploited to the fullest. Common approaches to control and thereby optimize the power output are tip speed variation, stall, variable blade pitch and yaw.

A wind turbine is designed for a rated wind speed for the most frequent operational condition. If rated wind speed is exceeded, the power has to be limited. The rotor blades are not designed for extreme rotational torques (turning force) or speeds, and it will literally tear the turbine apart. Therefore, any wind speed below or above the rated wind speed; power regulations are needed to prevent the rotor from fatigue loads and undesired performance.

For good turbine performance, the separation of flow on the blades should be avoided. To prevent this from happening, the blades are twisted slightly, so that the rotor blades stall gradually. This is called *passive stall control*. When wind speeds exceed the rated wind speed, the angle of attack will increase, until it starts to stall at some point. The large angle of attack

creates turbulence on the side of the rotor blade, and the stall prevents the lift force from acting on the rotor. [4] By using this control, high loads and high power production that can cause problems to the electrical motors are avoided. This is a passive type of power control, as the angle of attack increase with increased wind speed. [5]

A common active aerodynamic control is the so-called *pitch control*. Pitch-regulated wind turbines have an active control system that is able to vary the pitch angle (turn the blade around its own axis) of the blades in order to decrease the torque produced, as illustrated in Figure 2.3. Active pitch control is constantly checking the power output several times per second. When the power output becomes too high, the blades are pitched slightly out of the wind. The angle of attack is then decreasing, resulting in a decrease in torque for a fixed-speed turbine and a decrease in rotational speed in variable-speed turbines. When the wind drops again, the blades are turned back into the wind. [4] During normal operation the blades will be pitched a few degrees every time the wind changes, to obtain maximum power output at all times.

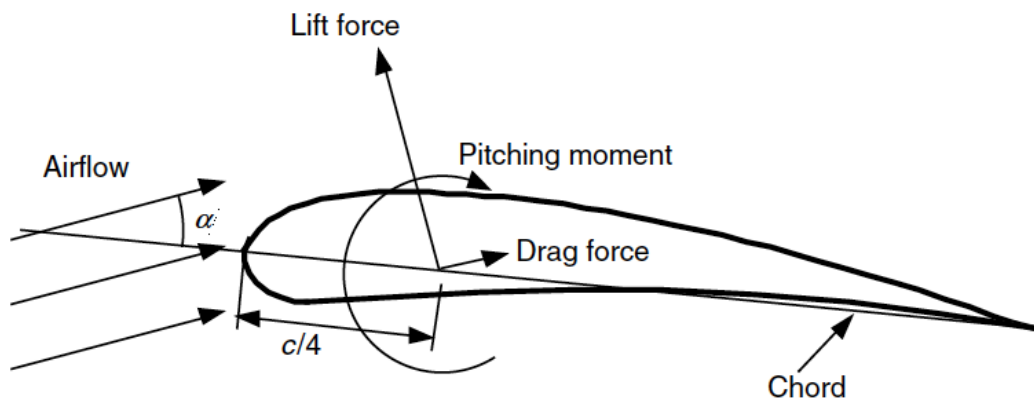


Figure 2.3 – Cross section of a rotor blade with pitching moment [1]

On larger wind turbines *active stall control* is more common, which is a combination of stall and pitch. In order to get a reasonably large torque at low wind speeds, the blades are pitched like a pitch-controlled wind turbine at low wind speeds. When the turbine reaches its rated power, the blades are pitched in the opposite direction from what pitch-controlled turbines are. [4] This will increase the angle of attack, making the blades go into a deeper stall. The advantages of pitch-controlled turbines are that it is possible to control the power output more accurately, and it will not get the same power drop as passive stall, as illustrated in Figure 2.4.

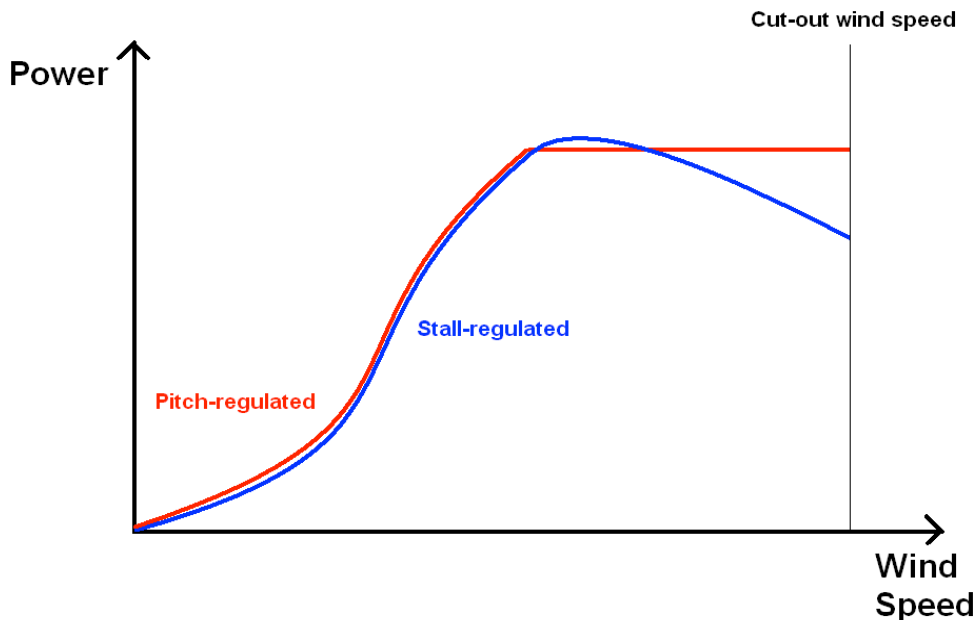


Figure 2.4 – Power curve of a pitch and stall-regulated wind turbine [6]

To maximize the power output the wind turbine should be perpendicular to the wind inflow. When the wind direction is perpendicular to the rotor, the rotor swept area is greater, hence more energy is captured in the wind and a lower amount of fatigue loads acts on the rotor. An important aerodynamic control is therefore *yaw control*, making it possible to turn the wind turbine towards the wind as the wind direction changes. The rotor is turned towards the wind by electrical motors, moving the entire nacelle around the tower. The yaw mechanism will be discussed more thorough in section 3.3.

2.3.2 Tip speed ratio

Another essential concept related to the power of wind turbines is finding the optimal tip speed ratio. Wind turbines must be designed to operate at their optimal wind tip speed ratio in order to extract as much power as possible from the wind stream.

The tip speed ratio (TSR) is defined as the ratio between the rotational speed of the tip of the blade and the actual wind speed velocity:

$$TSR = \lambda = \frac{\omega r}{U} \quad (2.17)$$

Where ω is the angular velocity, r is the radius of the blades and U is the free stream velocity.

If a rotor rotates too slowly, most of the wind will pass through the turbine undisturbed without being captured by the blades, and thus does not extract as much energy from the wind compared to its potential. When the rotor blade passes through the air stream it leaves a turbulent wake on its path. For this reason, if the blades spin too fast, they will be spinning through the “used” turbulent wind, which creates a large amount of drag. The rotor will then appear as a solid wall to the wind, as it will block the wind from passing through. The tip speed ratio depends on the airfoil profile used for the blades, number of blades and wind turbine type. [7]

In general, a high λ is desirable, which allows for efficient operation of an electrical generator. The higher tip speed ratio, the closer the power coefficient can approach the theoretical maximum.

Figure 2.5 shows how the power coefficient of an ideal wind turbine increases with the tip speed ratio in a case with wake rotation, and at the same time approach the maximum theoretical maximum from Betz limit.

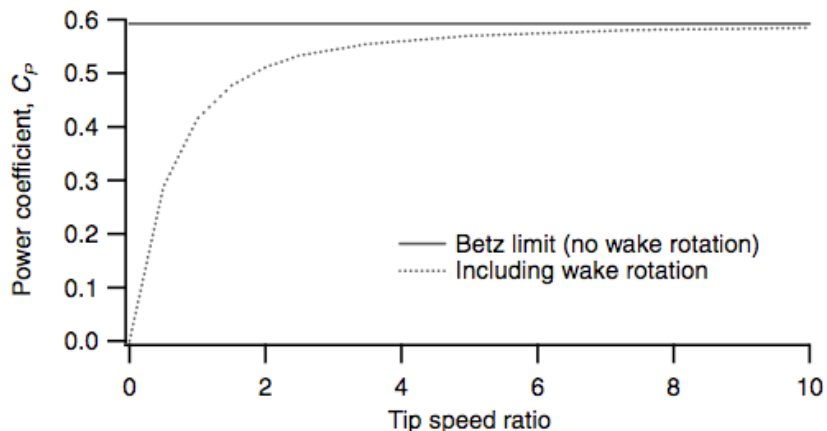


Figure 2.5 – Theoretical maximum power coefficient as a function of tip speed ratio for an ideal wind turbine, with and without wake rotation. [1]

Although a high tip speed ratio is desirable, it comes with certain disadvantages such as noise, vibration, reduced rotor efficiency due to drag and tip losses. These disadvantages need to be taken into account when finding the optimal tip speed ratio.

3 Wind and wakes

Theory on wind turbine wakes will be introduced in the following.

3.1 Wind turbine wakes and turbulence

The major challenge with wind power is the losses from the wake rotation that occurs behind a rotating turbine. The wake rotation will affect both the turbine producing the wake and other turbines downstream in a wind farm. When a wind turbine rotates, the rotor generates angular momentum, which is associated with torque. Due to the exertion of torque on a turbine's rotor created by the wind passing through it, an equal and opposite torque is imposed on the air, called "reaction-torque". This reaction torque causes the flow behind the rotor to rotate in the opposite direction of the rotor blades. The generation of rotational kinetic energy in the wake results in less energy extracted by the rotor, compared to what would have been without the wake rotation.

The wake of a turbine is often thought of as consisting of a near wake and a far wake. The near wake is within the region of approximately one to three rotor diameters downstream of the rotor, where the turbine geometry determines the shape of the flow field. Because of the turbulence and vortices generated at the rotor, much of the natural periodic flow is lost in the near wake. However, the far wake results in much more evenly distributed turbulence and velocity profiles, because mixing of the flow in the near wake with the free stream flow slowly re-energize the flow. [1].

The turbine rotor blades are one of the major sources of turbulence in a wake. Each rotor blade generates a sheet of vortices from the trailing edge of the blade that is transferred through the wake by the rotational flow in the wake. In addition, each blade also generates vortices at the tip of the blade, which is created by the pressure difference between the lower and upper side at the tip of each rotor blade. The tip-vortices of each blade tip follow a helical path, and as they travel downstream they start to merge. The merged vortices create a shear layer separating the slower moving flow inside the wake from the free stream outside the wake. However, the turbulence in the wake acts like an efficient mixer; it mixes the low velocity flow with the high velocity flow outside the wake. This causes the shear layer to grow with downstream distance, and eventually, it will reach the center of the wake, see Figure 3.1. As the interior of the wake is mixed with the free stream velocity, momentum is transferred into the wake, causing the wake to expand, and at the same time reducing the velocity deficit. In Figure 3.1 there is an illustration of the near and far wake behind a wind turbine, where it can be seen that the velocity deficit is decreasing with distance.

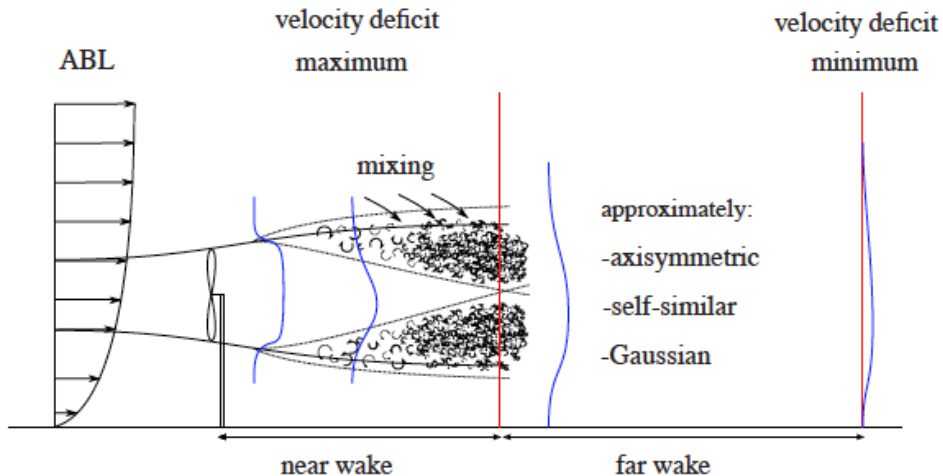


Figure 3.1 – Velocity profile in the wake of a turbine [8]

Other sources of turbulence are the presence of the nacelle and tower disturbing the airflow as well as the natural turbulence existing in the atmosphere. The mechanical turbulence (presence of the nacelle and tower) is of high frequency and will die out relatively fast. The tip vortices present in the shear layer will have broken down within the region of approximately 4 D. [9].

3.1.1 Turbulence intensity

Wakes of horizontal-axis wind turbines are complex turbulent flow structures. Turbulent flow does not have a defined value, as compared to laminar flow. The velocity will vary continuously as a function of time and space, because of both fast and slow varying fluctuations over time. The most important characteristic of turbulence is probably its randomness. For this reason, it is not easy to define turbulence, and impossible to calculate all the different flow variables at all times in each position. To predict mean velocities and say something about the statistical content in the movements are therefore satisfying. This led Osbourne Reynolds in 1895 to rewrite the continuity and momentum equation in terms of time-averaged turbulent variables, by introducing a new fluctuating quantity. [10]

The instantaneous flow was then separated in one mean velocity and one fluctuating velocity, expressed by:

$$U_i(t) = \bar{U}_i + u'_i(t) \quad (3.1)$$

where i is the direction of the velocity components, $U(t)$ is the instantaneous velocity consisting of a mean velocity, \bar{U} , and a time-dependent fluctuating velocity, $u'_i(t)$.

Turbulent flows are governed by the Navier-Stokes equations, as it is believed that any kind of flow may be described by the general Navier-Stokes equations. An approach based on a statistical description of turbulence may therefore be derived using the Navier-Stokes equations, together with the flow variable separated by a mean and a fluctuating quantity. The Reynolds-averaged Navier-Stokes equations will not be derived in this report, but can be found in White: Viscous Fluid Flow [11].

In the Reynolds-averaged Navier-Stokes equations, the turbulence kinetic energy can be calculated by closing the system of mean flow equations, which is referred to as a turbulence model. [12] In general, the turbulence kinetic energy can be expressed by the fluctuating quantity (also referred to as normal stress) as:

$$E_k = \frac{1}{2}(u'_1^2 + u'_2^2 + u'_3^2) \quad (3.2)$$

It is important to remember that turbulent flow is three-dimensional. During the present study one hot-wire was applied for the wake measurements, thus only the normal stress component in the average flow direction, u'_1^2 , was obtained. By assuming the vortices in the turbulent air consist of vortices with three components of equal magnitude, u'_1^2 will represent one third of the turbulence kinetic energy produced. Thereby, only one velocity component may still be used to characterize the turbulence kinetic energy produced by the wake at different positions.

Turbulence intensity is defined as

$$I = \frac{\sigma}{\bar{U}} = \frac{\sqrt{u'^2}}{\bar{U}} \quad (3.3)$$

where σ is the standard deviation of the wind velocity in the average wind direction, and \bar{U} is the magnitude of the mean wind velocity.

3.2 Wake interference in wind farms

The most obvious effects of wake interaction in wind farms are the velocity deficit and increased turbulence causing higher loads on turbines downstream in an array. As wind flows through a turbine, the air downwind of the turbine has a lower wind speed and higher turbulence than the free stream wind, as illustrated in Figure 3.2.



Figure 3.2 – Wake behind wind turbines in an array[13]

Because wind turbines are most effective in a steady wind without significant changes in the wind direction, the chaos in the wake will naturally cause less production for the wind turbines that are downwind of others. However, when there are several rows in a wind farm, the wake of a downstream turbine recovers more quickly than the one upstream. This is due to the increased turbulence levels created by the upstream turbines that lead to better turbulent mixing and faster velocity field recovering for downstream turbines. The second turbine in the row experiences the greatest power loss, while successive turbines experience decreasing power loss between each turbine farther down in the row. [8]

It is difficult to calculate the exact losses caused by this phenomenon, and it is usually applied a wind forecasting design tool together with appropriate wake models. However, the wake modeling software is still in a relatively early stage, and it will continue to develop. [14]

The wind turbines will be positioned with a certain distance apart from each other, depending on the diameter of the rotors. Decay in a wake is a function of the distance behind the turbine generating the wake, and by optimizing the geometry of the wind farm the array losses can be reduced. The further away a downwind turbine is located from an upwind turbine, the less impact it experiences in terms of wake losses. At the same time, total area used for the wind farm needs to be considered. Studies have shown that by spacing the downwind turbines 8-10 rotor diameters apart; array losses may be reduced to less than 10%. [1]

Also, by placing the turbines in the same row closer together, the turbulence and wake are reduced. Normally this will be between 2 to 3 times the rotor diameters. [15]

3.3 Effect of yaw

To maximize the power output a wind turbine should be perpendicular to the wind inflow. When the wind direction is perpendicular to the rotor, the rotor swept area is greater, hence more energy is captured in the wind, and a lower amount of fatigue loads acts on the rotor. As the wind direction changes, the incoming wind will be oblique in some periods of operation. There will then be a misalignment between the wind and the turbine pointing direction, referred to as the yaw angle, shown in Figure 3.3.

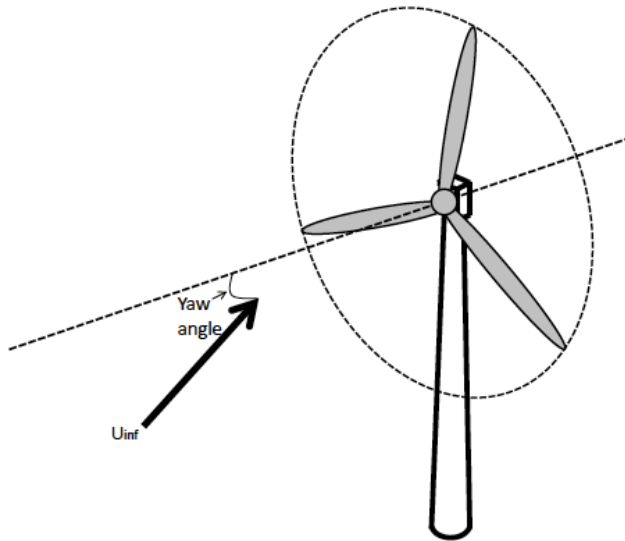


Figure 3.3 – Yawed turbine with yaw angle, γ . [16].

When the wind turbine is misaligned with the wind direction, fluctuations such as blade arc, angle of attack, lift and drag will occur. When the turbine rotates while operating in yawed conditions, the angle of attack on each blade is continuously changing, resulting in fluctuating loads on the rotor blades, which eventually will cause fatigue damage and affect the lifetime of the wind turbine. The most extreme fluctuations will occur at the top and the bottom of the blade path. This will cause the wind turbine blades to move partially in and out of the wake and the incoming flow, resulting in non-symmetrical loads acting on the turbine.

Due to the variability of the wind direction outside in the free, today most modern turbines have a yaw system, ensuring that the turbine faces the wind at all times during operation. The rotor is turned towards the wind by electrical motors, moving the entire nacelle around the tower. If the yaw system is actively controlling the yaw angle, the turbines may experience wearing and also reduced lifetime, something that needs to be considered. [17]

By minimizing the yaw angle, the power output is maximized and non-symmetrical loads are minimized. Evidently, this is desirable for one individual turbine, but in a wind farm

consisting of several wind turbines it may be favorable to yaw upstream turbines, to obtain a better efficiency of the downstream turbines and also overall efficiency.

3.3.1 Momentum theory for a wind turbine operating in yaw

Deriving a theoretical estimate of power production to a yawed turbine is somewhat difficult. The momentum theory is only applicable for determining an average induced velocity for the whole actuator disk, which is not the case for a yawed rotor. Once the turbine rotor is misaligned with the wind direction, blade circulations will cause the induced velocity to vary both in radial and azimuthal direction (the circular blade path). However, in the non-yawed case the momentum theory does allow some variation in the radial direction, but not in the azimuthal direction. By assuming that the force acting on the rotor disk (which is normal to the rotor disk) is responsible for the rate of change of the flow, the induced velocity will also be in the direction of the yawed rotor disk plane, thus the axial direction. [18] The induced velocity will therefore be directed at a yaw angle to the free stream wind direction, and the wake will be deflected to one side depending on what direction the turbine is yawed, see Figure 3.4.

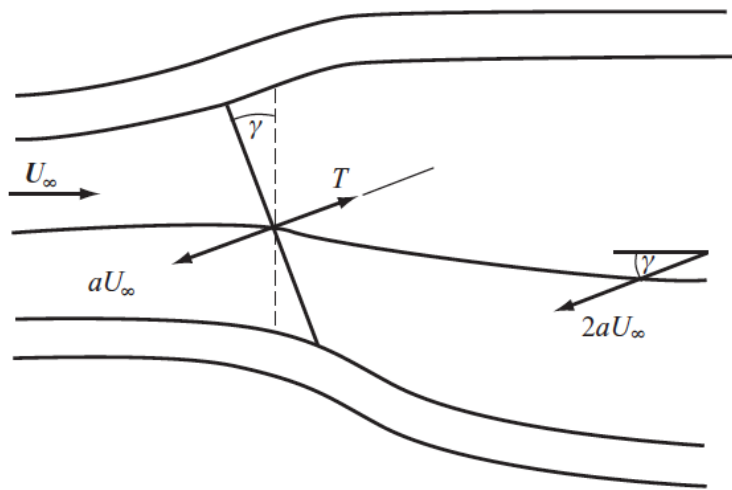


Figure 3.4 – Yawed inflow with skewed wake and induced velocities. [18]

By assuming that the rate of change of momentum in the axial direction is equal to the mass flow rate through the rotor disk times the change in velocity perpendicular to the rotor, the momentum equation can be expressed as

$$T = pAU(\cos\gamma - a)2aU \quad (3.4)$$

where the rotor axis is positioned at a yaw angle, γ , U is the free stream velocity, and a is the axial induction factor. The only difference between Eq. (3.4) and the un-yawed rotor disk theory yielding Eq.(2.15), is the part $(1 - a)$, which is here substituted with $(\cos\gamma - a)$. Using the same theory as for the un-yawed condition, the power can therefore simply be derived as

$$P = TU(\cos\gamma - a) \quad (3.5)$$

The power and thrust coefficients are then given by

$$C_P = 4a(\cos\gamma - a)^2 \quad (3.6)$$

$$C_T = 4a(\cos\gamma - a) \quad (3.7)$$

By differentiation, the maximum value of C_P can be found as

$$a = \frac{\cos\gamma}{3} \quad \text{and} \quad C_{P_{\max}} = \frac{16}{27} \cos^3 \gamma \quad (3.8)$$

A common estimation used for power prediction in yawed inflow is this $\cos^3\gamma$.

The power output of a turbine operating at a certain yaw angle is estimated to fall with $C_P(\gamma) = C_P(\gamma = 0)\cos^3(\gamma)$. This rough calculation may be useful as a control parameter in terms of yawing certain turbines to increase the total power output of a wind farm.

However, the momentum theory applied on a yawed rotor above may be satisfactory for determining the average axial induced velocity, but it may not be competent of determining the induced velocity at each blade element with good accuracy. The calculation of blade forces on a yawed turbine will not be further derived in the present study, as this is not the aim of the study.

3.3.2 Wake control and yawing

As mentioned previously, the wake contribution of upstream turbines can interfere significantly with the overall power output of a wind farm. Wind farms are often tightly clustered, large wind farms in particular, as the area of land usage is limited. Thus, performance will be affected. It is therefore advantageous to minimize the interaction between the wake from an upstream turbine and a downstream turbine. Yawing a turbine can therefore also be a method for actively controlling the direction of the wake, thereby controlling the power output of downstream turbines and decreasing loads. A useful method is therefore to selectively yaw upstream turbines in such a way that their wakes are deflected away from neighboring turbines. When the rotor plane is no longer perpendicular to the inflow, the wake will be asymmetric. Skewed wakes have the downwind part of the rotor closer to the wake centerline than the upwind part of the rotor, experiencing higher induced velocities and forces. The centerline of the wake will be at an angle χ to the axis of rotation, and is called the skew angle. The skew angle is greater than the yaw angle, and is illustrated in Figure 3.5, where the deflected vortex is also shown. For this reason, it is possible to control the wakes position by yawing the turbine. [8]

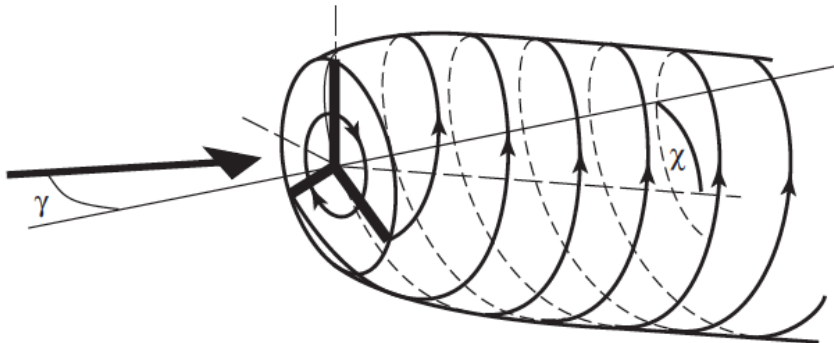


Figure 3.5 – The deflected vortex wake of a yawed turbine, with skew angle χ . [18]

While improving the performance of downstream turbines, the consequences for the yawed turbine will be reduced efficiency and eventually increased loads. Thus, a balance must be reached in order to maximize the power output from the wind farm as a whole. Obviously, the advantage of power increase for the downstream turbines ought to be greater than the power loss of the wake controlled turbines. Yaw can be a very important power control in wind farms, where not only one individual wake, but also several wakes most likely will interact.

4 Experimental set-up and methods

Experiments were conducted on the two model wind turbines in the wind tunnel. Necessary information on the experimental set-up as well as measurement techniques is presented in the following.

4.1 Wind tunnel and model turbines

The experiments in the present study were performed in the closed-return wind tunnel of the Department of Energy and Process Engineering at the Norwegian University of Science and Technology, Trondheim. The two turbines that are deployed have been developed for testing in this wind tunnel. A picture of the model turbines during the experiment is shown in Figure 4.1.



Figure 4.1 – The two wind turbine models in the wind tunnel

The test section of the wind tunnel has a height of 2 meters, a width of 2.71 meters and is 11.14 m long. The height of the wind tunnel may be increased to 2.3 m from the inlet to the outlet, so that the wall boundary layer growth can be accounted for. The air in the wind tunnel is generated by a fan of 220 kW, which is able to provide air velocities up to 30 m/s.

During this experiment, the upstream turbine was placed on a 6-component force balance, which has an accuracy of better than 0.5% when the turbine operates under design conditions, and a total thrust force error of less than 2%. [19] The scale can be rotated 360° with respect to the tunnel axis, making it possible to simply rotate the scale when the turbine is operating in yawed conditions. The wind tunnel is also equipped with a four-axis traversing system controlled by a computer, enabling measurements at all different positions desired. The axis in the test section is defined as illustrated in Figure 4.2, where the wind tunnel test section is seen from above.

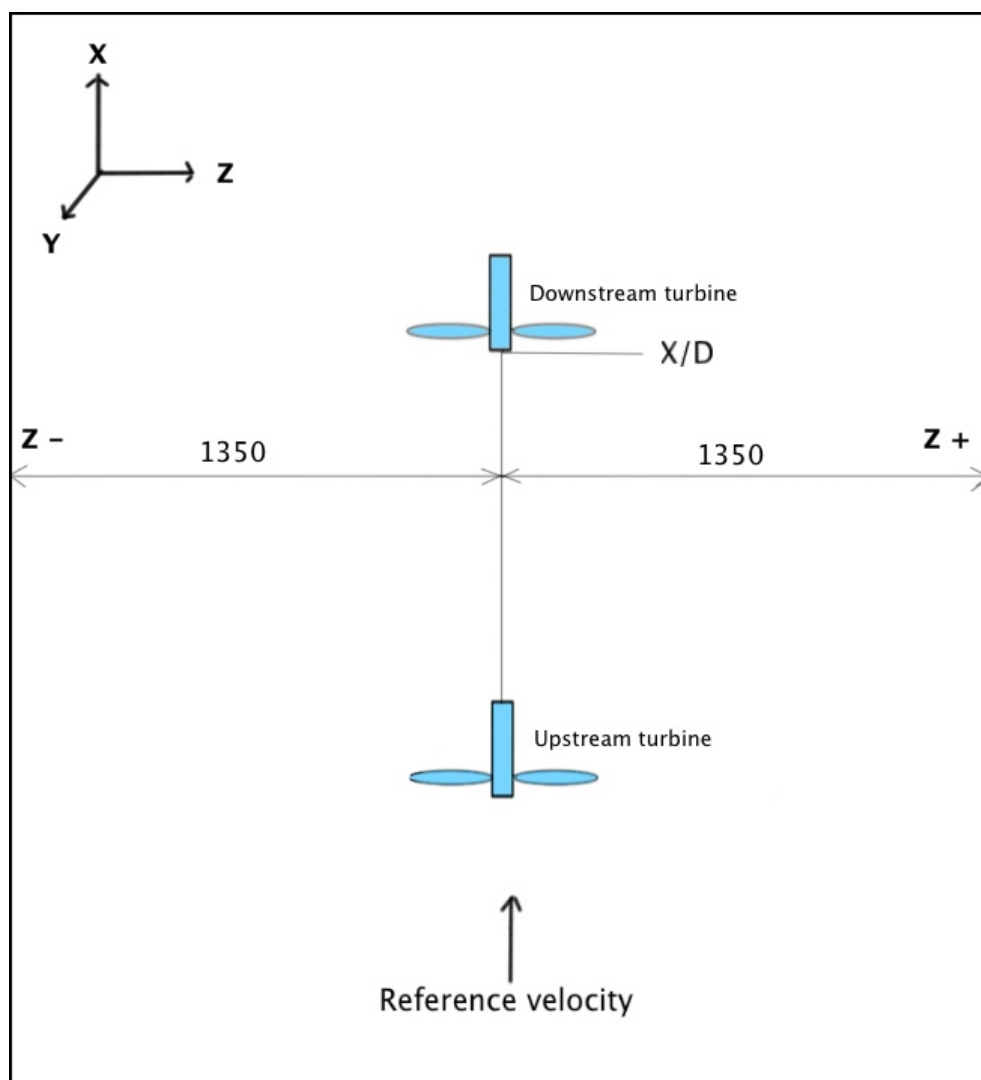


Figure 4.2 – The wind tunnel test section seen from above

The two model turbines are three bladed and have upstream rotors. Both turbines are driven by a belt transmission connected to a generator installed under the floor, and controlled by a frequency converter. For the first turbine, the belt is mounted inside the tower, and for the second turbine the belt is behind the turbine tower. The geometry of the turbines is the same, except for a slight difference in the rotor diameter. The diameter of the first turbine is 940 mm and the second turbine has a diameter of 900 mm. The height from the ground plane to the center of the hub is measured to be 817 mm for both turbines. More details on the blade geometry of the test model turbines are given in Krogstad and Karlsen. [20] The software LabVIEW is used to record the measurements in the experiment.

4.2 Scaling and blockage effects

The main advantage of doing measurements in a wind tunnel, as compared to field simulations, is the controlled wind flow providing essential data. Also, full-scale tests are very time-consuming and more expensive to carry out.

The two drawbacks of wind tunnel experiments are scaling and blockage effects. Scaling effect is the effect of scaling in order to represent the “real world”. To obtain a realistic simulation in a wind tunnel, both tip speed ratio and Reynolds number ought to be the same as for full-scale turbines. The tip speed ratio criteria can without difficulty be met, but the Reynolds number criteria is impossible to accomplish, as the difference in chord length is obvious and the wind speeds must be kept low to avoid too high rotational speeds. However, as long as an appropriate wing profile is chosen, of which the characteristics are known for the particular airfoil, measurements at low Reynolds numbers are suitable for comparison. [21] For reliable comparison of model tests with full-scale tests, a recommended minimum Reynolds number is of the order of $Re = 3 \times 10^5$. [22]

The blockage effect is the interference of the wind tunnel walls. Especially for high tip speed ratios, the rotor will appear as a flat disk blocking the wind from passing through, and the wind will flow around the blockage caused by the rotor spinning. If the blockage ratio is high enough, the effects of the tunnel walls may interfere with the flow, as the wind will not be able to spread out as much as it would without the presence of the walls. As a result of this, the wind speed between the walls and the “flat disc” area will exceed the free stream velocity. The two models used for the present study have small differences in the rotor diameters, resulting in a slightly different blockage ratio. The two blockage ratios are about 11.8% and 12.8%, and are defined as the rotor swept area divided by the cross-sectional area of the wind tunnel. This is close to the recommended upper limit of 10%, in order to avoid wall interference on the measurements. [22]

4.3 Measurement techniques

Two different measurement techniques for the wake profiles were used in this experiment. Some of the measurements were done using a pitot tube, which is a tool for measuring mean velocity. When it was desirable to obtain more details of the wakes in terms of turbulence intensity, a hot-wire anemometry was applied.

4.3.1 Pitot-static tube

A pitot-static tube, also referred to as a Prandtl tube, is a pressure measurement tool used to measure fluid flow velocity. The basic principle of the instrument is to measure the pressure difference between the total pressure and the static pressure, making it possible to calculate the mean velocity. There is a center hole in the axis of the tube always pointing in the direction of the flow, and several small holes outside of the tube perpendicular to the center tube, illustrated in Figure 4.3.

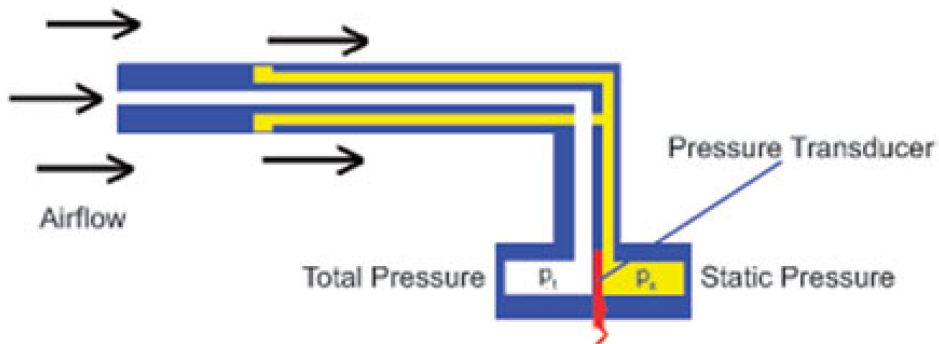


Figure 4.3 – Pitot-static tube. [23]

A pressure transducer is connected to the outside holes at one side and to the center hole at the other side. The pressure transducer measures the strain in a thin element using an electronic strain gauge to find the pressure difference between the center hole and the outside holes, hence the difference between p_{tot} and p_s . [24] Knowing that the dynamic pressure is the difference between the total and static pressure and also knowing the local air density, the mean velocity in the flow can be found from Bernoulli's equation as

$$p_s + \frac{1}{2} \rho U^2 = p_{tot} \quad (4.1)$$

Solving for U , the following expression is used for calculating the mean velocity:

$$U = \sqrt{\frac{2(p_{tot} - p_s)}{\rho}} \quad (4.2)$$

4.3.2 Hot-wire anemometer

A hot wire anemometer is a technique for measuring velocity up to high frequency fluctuations. Its ability to detect and follow fast velocity fluctuations is one of the major reasons for using a hot wire anemometer. For this reason, hot-wire anemometry is an appropriate technique for measuring velocity fluctuations in turbulent flow.

The hot wire anemometry consists of a sensor, a very fine wire, and of electronic equipment making it possible to transform the sensor output into a valuable electrical signal. The wire is electrically heated to 100-200 degrees above ambient temperature while it is exposed to the airflow. [5] As the wire possesses a higher temperature than the air flowing past the wire, convection will occur, where heat is transferred from the heated wire to the cold surrounding flow. As heat transfer is a function of fluid velocity, a relationship between the velocity and the electrical signal can be made. [25] There are two main methods for implementing hot wire anemometers. Either by providing a controlled amount of electrical current in the wire, constant-current anemometer (CCA), or keeping the temperature of the wire constant, constant-temperature anemometer (CTA). The latter is by far the most employed method, and is used in this experiment. [26] The dimensions of a typical hot wire probe are 5 μm in diameter with a length of 1-3 mm, where an illustration of the wire is seen in Figure 4.4.

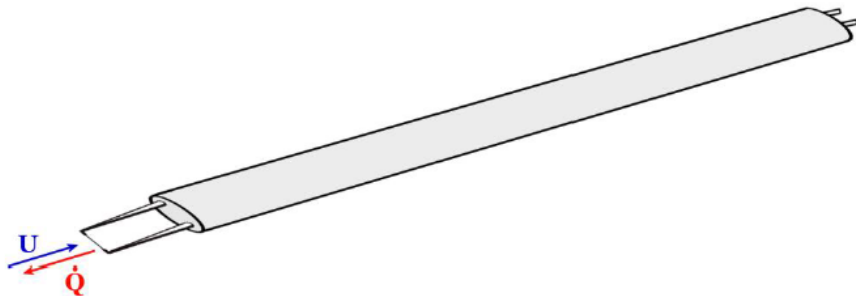


Figure 4.4 – Hot-wire probe. [27]

The steady state energy balance of a hot wire is expressed by:

$$W = Q = I^2 R_w = h A (T_w - T_a) \quad (4.3)$$

Where W is the power generated by heating and Q is the convective heat transfer from the wire. I is the heating current flowing in the wire, R_w is the wire resistance operating at temperature T_w , A is the area of the wire, and h is the heat transfer coefficient.

From the energy balance it is apparent that the voltage is dependent on the convective heat transfer to the surrounding fluid.

In constant-temperature anemometry (CTA), the wire is the fourth arm of a Wheatstone bridge. Its resistance changes depending on the local speed experienced, and so does the voltage needed to balance the bridge. When the bridge is in balance, there is no voltage difference over the bridge. If the local flow velocity increases, the wire resistance will decrease, and a voltage difference over the bridge will occur. The voltage difference in the current will then regulate the amplifier, resulting in an increase in the current supplied to the wire, which will also increase the wire resistance until the Wheatstone bridge is balanced again.

The electric circuit is shown in Figure 4.5, where the amplifier output E required for maintaining a constant temperature in the wire is a function of the velocity.

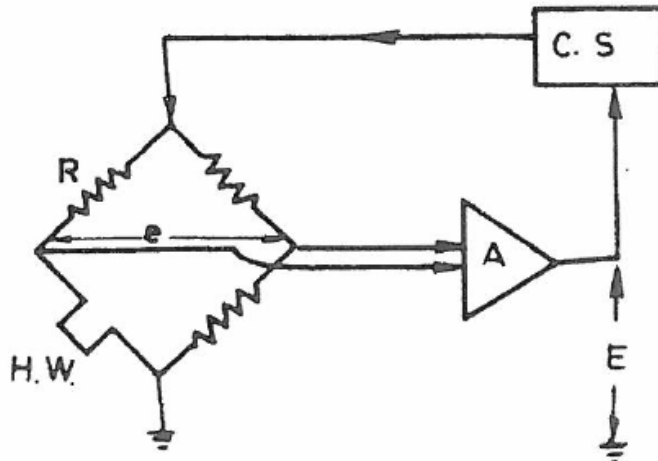


Figure 4.5 – Constant temperature control circuit [25]

The law describing the relation between the velocity and the voltage for one-component velocity measurements is known as the modified King's Law:

$$U = \kappa_1 (E^2 - E_0^2)^{\frac{1}{n}} + \kappa_2 \sqrt{E - E_0} \quad (4.4)$$

where E is the measured voltage, E_0 is the voltage at zero velocity and κ_1 , κ_2 and n are constants from the calibration.

Before the measurements can be conducted, the resistance in the hot-wire, $R_{\text{wire},h}$, required to keep the temperature constant at a desired value needs to be found. As the resistance in the wire is a function of the temperature, the resistance needs to be held constant as well. The resistance is found from the following relations:

$$\beta = 1 + \alpha(T_{\text{wire}} + T_{\infty}) \quad (4.5)$$

$$R_{\text{wire},h} = \beta(R_{\text{wire},c} + R_{\text{cable}}) - R_{\text{cable}} \quad (4.6)$$

The first relation represents the overheating factor, β . T_{wire} is the wire temperature, T_{∞} is the room temperature and α is the temperature coefficient of the wire material. The material of the wire used in this experiment is of platinum covered with 10% rhodium, thus $\alpha = 1.69 \times 10^{-3}$. When the overheating factor is found, the resistance in the hot wire, $R_{\text{wire},h}$, can be found from Eq. (4.6). $R_{\text{wire},c}$ is the resistance in the wire before it is heated, and is given by the specific hot-wire characteristics. R_{cable} represents the resistance in the cable, and is found by measuring the total resistance of the wire and the cable by connecting the wire to a multimeter. When the resistance of the wire is calculated to attain the desired wire temperature, this wire resistance is put into the anemometer.

Hot-wire exercise on pipe flow

Prior to the experiments made in the wind tunnel, an experiment using hot-wire anemometry to obtain a cross-sectional velocity profile in a pipe was conducted. This was mainly done to get experience using hot-wire as a measurement tool, obtaining more knowledge of how they work and understanding the results. The hot-wire measurements were carried out for positions from the center to the wall of the pipe (approximately one radius, horizontally). This was conducted by orienting the probe wire both horizontally and vertically, to see if the orientation has any effect on the results. Some calculations were required to plot the results in terms of turbulence intensity.

The turbulence is represented by the normal stress component u'^2 , as introduced in the previous section. The normal stress is normalized by the reference velocity in the pipe, which is called the friction velocity, u^* . The friction velocity is found from the following relations for turbulent pipe flow:

$$U_{avg} = \frac{Q}{A} = \frac{1}{A} \int_0^R 2\pi r \times u(r) \times dr \quad (4.7)$$

$$Re_D = \frac{U_{avg} D}{v} \quad (4.8)$$

$$f = 0.316 Re_D^{-\frac{1}{4}} \quad (4.9)$$

$$u^* = \sqrt{\frac{f \times U_{avg}^2}{8}} \quad (4.10)$$

The average velocity in the pipe, U_{avg} , was found from Eq. (4.7). Further, the Reynolds number was calculated to be greater than 4000, which means that the turbulent flow is fully developed. The Darcy friction factor, f , was calculated from Eq. (4.9), making it possible to find the friction velocity, u^* , from Eq. (4.10). The normal stress was then normalized by u^{*2} , to obtain a dimensionless quantity of the turbulence intensity.

Figure 4.6 and Figure 4.7 show the results from the pipe flow measurements, where the mean velocity profile and the turbulence intensity are presented, respectively.

The mean velocity is non-dimensionalized by the maximum velocity measured in the pipe, and the different positions are normalized with the pipe radius. Hence, $y/R = 1$ represents the center of the pipe.

The mean velocity is decreasing closer to the wall of the pipe as expected, due to the wall interfering with the flow causing higher turbulence intensities. This corresponds to the

increasing turbulence level when moving closer to wall, see Figure 4.7. In the center of the pipe, the mean velocity does not interfere with the wall, and the velocity here reaches its maximum, while the turbulence level reaches its minimum. The effect of the probe orientation seems to be minimal.

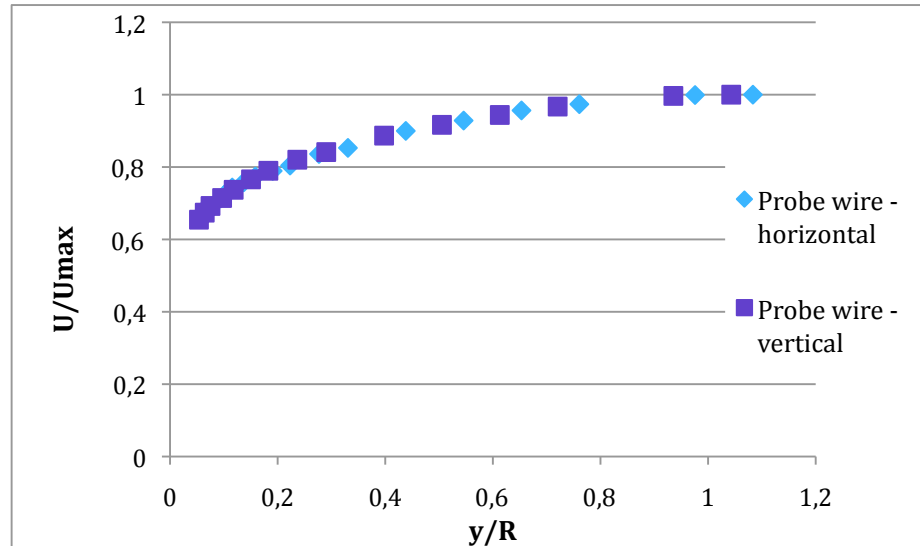


Figure 4.6 – Horizontal mean velocity profile of the pipe's cross-section.

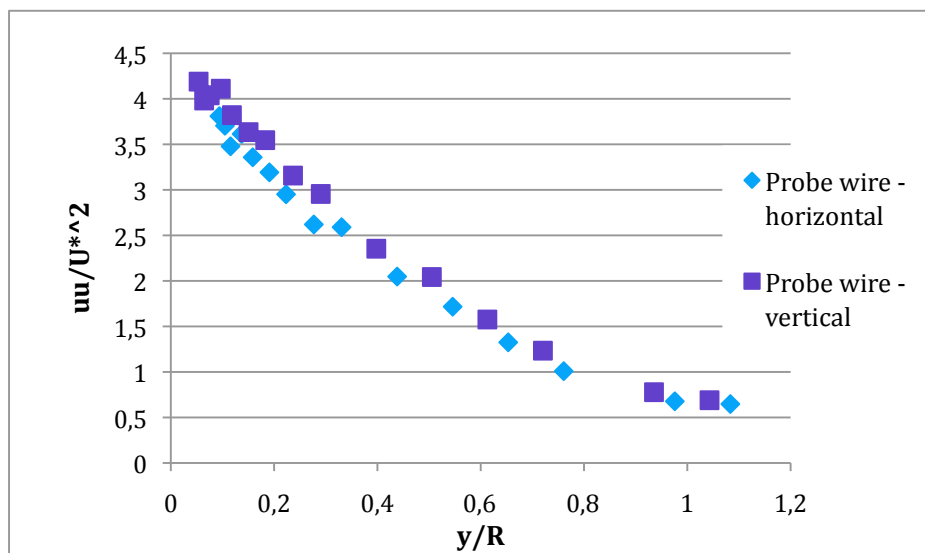


Figure 4.7 - Horizontal turbulent velocity profile of the pipe's cross-section, in the average flow direction.

4.4 Calibration

Calibration was done for all measurements to obtain an accurate relation between the sensor signals and the forces acting on the turbines. Prior to each experiment, the instruments were calibrated to obtain the most accurate results possible.

In addition to the calibration, it was necessary to find the atmospheric pressure for each day working in the laboratory, as this is needed for the calculations. This is found by reading the height of mercury in mm off a mercury column together with the temperature. From this, it is possible to find the air density from the ideal gas law.

$$p = \rho_{Hg}gh \quad (4.11)$$

$$\rho_{air} = \frac{p}{RT_{avg}} \quad (4.12)$$

From the pressure equation of liquid, the pressure is found using measured mmHg with the density of mercury. Subsequently, the air density was found from the ideal gas law, eq. (4.12), where R is the ideal gas constant of 286.7 and T_{avg} is the average temperature in Kelvin.

4.4.1 Torque

The torque force was calibrated using different weight elements with known mass. By calculations and linear regression, an accurate relation between the sensor signals and the real force acting on the turbine was obtained.

Seven small weights up to 466 grams were applied on the tip of the rotor blade. This resulted in a maximum moment of 2 Nm, which is about maximum of what the turbine can withstand. The moment acting on the shaft was calculated for each weight element from the torque relation $F_T = m \times g \times arm$, where the arm was measured to be 0.45 meters. The calculated torques were then plotted against the voltage signal, resulting in a constant with units $\left[\frac{Nm}{V} \right]$.

From the torque voltage signal and the calibration constant, the power and the power coefficient can be found directly from the two relations

$$C_P = \frac{P}{\frac{1}{2} \rho A U^3} \quad P = F_T \times \omega \quad (4.13)$$

4.4.2 Thrust

The thrust force was also calibrated using different weight elements with known mass.

Masses up to almost 6 kg were applied on the scale the turbine was placed on, resulting in a maximum thrust force of approximately 60N. The thrust force acting on the turbine was calculated for each weight element from Newton's second law, $T = m \times g$, where T is the thrust force, m is the mass and g is the gravitational acceleration. The thrust force was then plotted against the voltage signal, resulting in a constant with units $\left[\frac{V}{N} \right]$.

From the thrust force, the thrust coefficient is found directly from the relation

$$C_T = \frac{T}{\frac{1}{2} \rho A U^2} \quad (4.14)$$

4.4.3 Pressure transducers

The contraction and the pitot-static tube used for wake measurements were each connected to a pressure transducer, manometer and amplifier. The pressure transducers were calibrated, obtaining constants for the contraction and the pitot-static tube, both in units $\left[\frac{Pa}{V} \right]$.

The manometer is the instrument used for calibrating the pressure transducers, and is a simple construction containing methylated spirit. As the airflow pressure increases, the methylated spirit pillar also increases. From the following relations, it is possible to calculate the pressure in the airflow and the resulting velocities:

$$p = \rho g h_{MethSp} \quad (4.15)$$

$$U = \sqrt{\frac{2 \Delta p}{\rho_{air}}} \quad (4.16)$$

4.4.4 Hot-wire anemometer

The hot-wire probe used for wake measurements were connected to an anemometer, an amplifier and an oscilloscope. The hot-wire anemometer was calibrated in the free stream region against a pitot-static probe, while the wind velocities were varied. The calibration of the hot-wire anemometer was carried out approximately every hour, which is necessary to obtain reliable results. The calibration curve for a hot-wire is non-linear, which makes it different from the other equipment calibrated in the present study. The pitot-static tube was placed next to the hot-wire probe in the wind tunnel, to obtain the mean flow velocities. The mean flow velocities were calculated from the pressure difference. Further, the mean flow velocity was plotted against the voltage signal from the hot-wire probe. The number of calibration constants is depending on the degree of the polynomial fit chosen, and is in units $\left[\frac{m/s}{V} \right]$.

The calibration curve as well as the calibration constants were plotted and found manually for the experiment conducted in the pipe prior to the wind tunnel experiments. The calibration constants and other parameters from the wind tunnel experiment were found using a programmed Fortran routine, which also temperature-corrected the recorded data. Information on mean, maximum and minimum velocities, as well as normal stress was given directly as output data from the Fortran program.

Further information on the calibration data as well as calibration curves can be found in Appendix A.

4.5 Measurement inaccuracies

There will always be some uncertainty and inaccuracies connected to experimental results. To obtain the different yaw angles, the balance was rotated manually. The different yaw angles were calculated, measured and marked on the balance by hand. This includes several small inaccuracies, since the balance was rotated using eye measurement every day for each experiment. The turbine was rotated around a vertical axis close to the center of the rotor, but there was a slight deviation between the rotation centerline and the center of the rotor. The reason for this was that it was not possible to move the turbine further back without drilling a new hole in the tunnel floor. The center of the rotor was 8.4 cm from the center of the balance, resulting in an arm that may cause some inaccuracies that needs to be taken into account. Also, the placement of the equipment, such as the two wind turbines and the two probes were measured by hand to find the right positions and to face them in the right directions. Inaccuracies linked to the calibration of the pressure transducers when using the fluid column manometer may also occur. During the calibration, the methylated spirit was not completely steady for each measuring point, and an approximate value had to be chosen.

In addition to human errors, the measuring instruments may give inaccurate results for many reasons. Variations in temperature or atmospheric pressure are two factors that may affect the results. All the measurements were checked before they were recorded, so if some of the results deviated more than others, one more measurement was made for comparison. During the wake measurements conducted with a pitot tube, 4 measurements were made in the center of the rotor for each 9 scenarios, where two of the four measurements for each scenario were computed on a different day. The errors of the four measurements were found to lie in between 0.06% – 3%, giving an average error of 1.5%.

5 Procedure

Within this study a number of test runs on the two model wind turbines in the wind tunnel were performed. A short description on how the different experiments were conducted is presented in this section. During the experiments, both turbines were spinning counter clockwise. In the present study, a positive yaw angle indicates that the right hand side (RHS) blade of the turbine was yawed upstream when viewed in the downstream direction, as seen in Figure 5.1. The pitch angles for both turbines were set to zero, and the upstream turbine was operating at constant tip speed ratio of $\lambda=6$ (design condition) for this entire study. To obtain the different yaw angles for the upstream turbine, the scale balance was rotated manually.

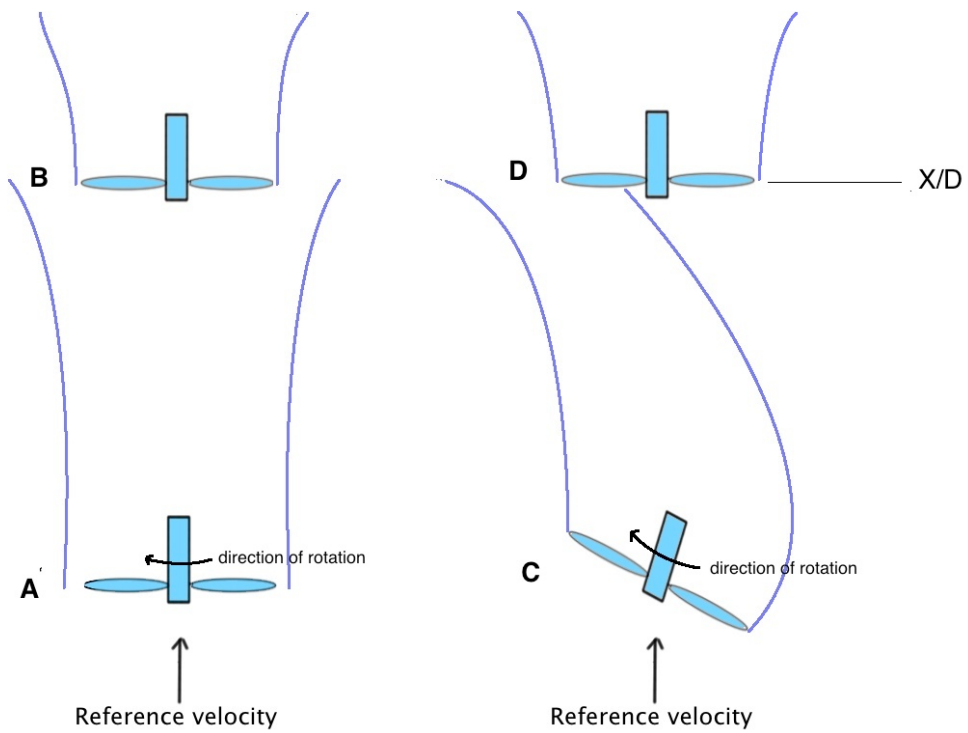


Figure 5.1 – Turbine B heavily disturbed by an un-yawed turbine A. By yawing turbine C, turbine D experience much less interaction with the wake produced.

In the zero yaw case the wake is expected to travel straight downstream of the rotor. When the turbine is positively yawed, the wake is expected to deflect towards the left hand side (LHS) of the rotor, as illustrated in Figure 5.1. When the RHS of the turbine is yawed upstream, a force from the LHS (which is normal to the wind) will act on the rotor, and an

opposite force from the RHS will act on the airflow, pushing the wind to the left. The degree of the deflection is strongly dependent on the yaw angle, and is expected to increase with increasing yaw angle.

5.1 Single model turbine operating in yaw

The single model turbine mounted upstream during the performance measurements and the downstream flow field measurements is the turbine with the larger rotor diameter, $D = 0.94$ m.

5.1.1 Performance

Performance measurements on the upstream turbine were carried out for the following yaw angles $\gamma = 0^\circ, 10^\circ, 20^\circ, 30^\circ, 40^\circ$ and 50° . Both turbines are equipped with torque sensors on their rotor shaft and RPM-sensors inside the hub. The power produced by the turbine can therefore be found directly from the relation $P = \omega \times F_T$, where F_T is the torque and ω is the angular velocity (RPM). The upstream turbine was placed on the force balance, which made it possible to measure the thrust force on the turbine. From the thrust force, the thrust coefficient can be calculated. A sampling frequency of 1000 Hz and a sampling time of 60 seconds were used, resulting in 60 000 samples for each measuring point. The time series was not recorded for this, as only the mean values are desired for these measurements.

5.1.2 Downstream flow field

The downstream flow field of the yawed turbine was studied in terms of mean velocities and turbulence intensities at hub height. The horizontal mean velocity profiles were carried out using a pitot probe at several different positions downstream while varying the yaw angles of the upstream turbine. The mean velocity profiles were obtained at three different positions downstream; $x/D = 1, 3$ and 4.78 , while the upstream turbine was operating at yaw angles of $\gamma = 0^\circ, 20^\circ$ and 40° , where x/D represents the distance from the rotor downstream in x-direction normalized with the diameter, D . The measurements for the horizontal mean velocity profiles were collected in a plane perpendicular to the mean flow direction (z -direction, see Figure 4.2). This was done with 100 mm steps, up to ± 1200 mm from the centerline of the rotor, leaving a distance of 150 mm to the wall, as it was not desired to measure inside the boundary layer. The same sampling frequency and sampling time used for the thrust and torque was also used for the pitot tube, which is adequate.

The turbulence intensity profiles were determined using a hot-wire probe connected to a

constant temperature anemometry (CTA) circuit, at 3D downstream of the upstream turbine operating at $\gamma = 0^\circ$, 20° and 40° .

The measurements on the turbulence intensity were collected in the same plane as for the mean velocity profiles, only in a tighter specter with smaller steps. The hot-wire was connected to an oscilloscope, which made it easy to see the peaks of the turbulence intensity. In addition, the locations for higher turbulence were already predicted from the horizontal mean velocity profiles. The measurements were collected step-wise down to 2 cm at locations of which the maximum turbulence was expected, to ensure that the highest level of turbulence was captured. When the turbulence intensities are measured with a hot-wire probe, a much higher frequency must be used, as it is desired to record a high frequency signal of a turbulent flow. A sampling frequency of 13 000 Hz and a sampling time of 60 seconds was used, resulting in 780 000 samples for each measuring point. The mean of the velocity and turbulence properties can then be acquired from the recorded time series over a time span of 60 seconds. Prior to the measurements, the wire resistance was calculated from the same equations as for the pipe flow exercise, Eq. 4.5 and 4.6.

Both probes were fastened to the traverse system, making it easy to move the probes along the cross-section of the tunnel, as well as for different positions downstream.

5.2 Wake interference on a second (downstream) model turbine

A second (downstream) turbine was mounted in line with the upstream turbine at 3D downstream. In this case, the turbine with the smaller rotor diameter, $D = 0.90\text{ m}$ was mounted upstream, and the turbine with the larger rotor diameter of $D = 0.94\text{ m}$ was mounted downstream. As the turbine characteristics are more or less the same, it should not obstruct the result to a significant extent.

5.2.1 Performance

The performance of the downstream turbine was measured when the upstream turbine was operating with yaw angles of $\gamma = 0^\circ, 10^\circ, 20^\circ, 30^\circ, 40^\circ$ and 50° . For each case, the power coefficient $C_p = P / \frac{1}{2}\rho A U_{ref}^2$ of the downstream turbine was found using the reference velocity seen by the upstream turbine, and was more or less constant to $U_{ref} \approx 10\text{ m/s}$ during all tests. The tip speed ratio for the downstream turbine is also based on the reference velocity seen by the upstream turbine.

5.2.2 Dynamic loads

The changes in dynamic loads (torque) experienced by the rotor blades of the downstream turbine while the upstream turbine was operating at varying yaw angles were also experimented on. The C_p -curves of the downstream turbine were obtained from the last measurements, for all the various yaw angles of the upstream turbine and were used to choose the measurement points for the dynamic load. Three points on each C_p -curve were chosen, the top point and one on each side, so that the dynamic loads could be evaluated when the downstream turbine was operating at its best. For each yaw angle of the upstream turbine ($\gamma = 0^\circ, 10^\circ, 20^\circ, 30^\circ, 40^\circ$ and 50°), three different tip speed ratios of the downstream turbine were therefore measured. A sampling frequency of 10 000 Hz and a sampling time of 30 seconds was used, resulting in 300 000 samples for each measuring point being used when examining the dynamic loads. Since the details of the dynamic load properties were desired and not only mean values, the time series were also recorded.

Computer software

A software program LabVIEW was used to record all the obtained data in the computer. After the data obtained from the hot-wire was recorded, a programmed FORTRAN routine was applied to temperature-correct the data and convert it to mean velocities and turbulence intensities. Finally, data evaluation and plots were completed using a combination of EXCEL and MATLAB, depending on the number of samples acquired.

5.3 Free stream velocity

At the inlet of the wind tunnel there is a contraction region, where the static and total pressures were measured at two different positions in the contraction region. To find the mean velocity in the flow, the conservation of mass can be applied:

$$U_1 A_1 = U_2 A_2 \quad (5.1)$$

From Bernoulli's equation along a streamline it is given that

$$\frac{1}{2} \rho U_1^2 + p_1 = \frac{1}{2} \rho U_2^2 + p_2 \quad (5.2)$$

By combining equation (4.1) and (4.2) and solving for U_2 an expression for the velocity at the inlet is following

$$U_2 = \sqrt{\frac{2\Delta p}{\rho \left(1 - \left(\frac{A_2}{A_1}\right)^2\right)}} \quad (5.3)$$

For this particular tunnel $1 - (A_2/A_1)^2 = 0.967$, and the pressure difference is measured with a pressure transducer.

U_2 is the velocity at the inlet. However, the free stream velocity at hub height experienced by the first turbine is the desired velocity. The correlation between the two velocities can be found either using the contraction region or placing a reference pitot where the center of the hub will be placed. For this report, a correlation found by Pål Egil Eriksen was used, so this was not preceded. The following correlation between the inlet velocity and the free stream velocity at hub height are applied on all measurements throughout this report:

$$U_{ref} = 0.2961 U_2 - 0.2143 \quad (5.4)$$

The free stream velocity used in the present experiment is $U_{ref} \approx 10$ m/s, requiring an inlet velocity of approximately $U_2 \approx 11$ m/s.

6 Results and discussion

The data collected from the experiments can be divided into three main groups: measurements performed on one single model turbine, the interactions between two turbines and a wind farm consisting of the two model turbines. The performance of a single upstream turbine operating at optimum λ with varying yaw angles is first presented in this section. Further, the aim is to understand to what extent the side force created by the yawed turbine affects the wake, thus the velocity deficits and turbulence intensities in the downstream flow field are presented. In addition, the performance and dynamic loads experienced by a second turbine operating at a position $x/D = 3$ downstream of the upstream turbine are also examined. Finally, the overall efficiency of the wind farm is presented for the different yaw scenarios.

6.1 Single model turbine operating in yaw

A single turbine operating at different yaw angles was investigated in terms of performance and its wake behavior at different positions downstream.

6.1.1 Performance

Firstly, it was interesting to examine the performance of the first (upstream) turbine operating at optimum tip speed ratio, λ , with different yaw angles, γ . The power curve and the thrust curve for the model turbine with zero yaw is shown in Figure 6.1, where it can be confirmed that design conditions is when operating at a tip speed ratio of 6, resulting in a maximum power coefficient of $C_P = 45.6\%$.

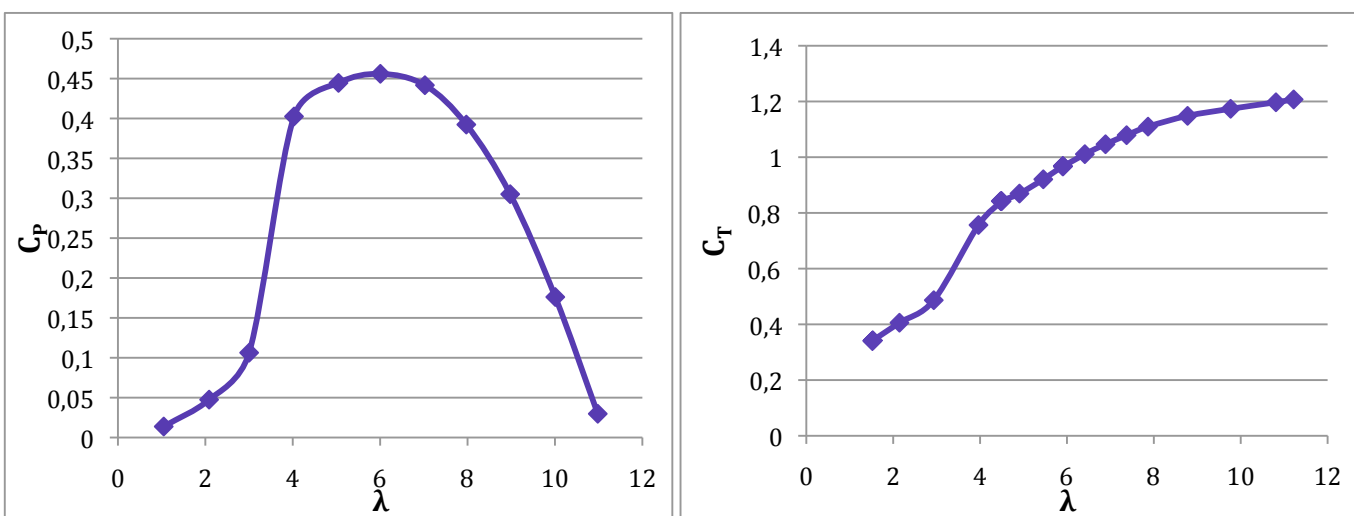


Figure 6.1 – Performance of the model turbine operating at zero yaw conditions

At tip speed ratios below the design condition, the blades experience a certain degree of stall, thus the power coefficient is decreasing with decreasing tip speed ratio. For tip speed ratios above the design condition, the power coefficient also decreases. This is due to the negative angle of attack experienced by the root of the blades, which causes the blades to provide power to the airflow instead of extracting the kinetic energy. For high tip speed ratios, the thrust coefficient is observed to exceed 1, which is not in accordance with Betz theory. According to Betz theory, the thrust coefficient is below one, as described on section 2.2. Since the model turbine is mounted inside a wind tunnel, the blockage effect due to the presence of the tunnel walls induce an increase in the velocity in front of the rotor, which also increases the thrust force acting on the rotor.

From earlier work [28], the optimal combination of operation of two turbines in an in-line arrangement was experimented on. It was proven that the upstream turbine should operate at design conditions ($\lambda=6$) in order to obtain optimal overall efficiency of the two turbines, practicing zero pitch and un-yawed conditions. For this reason, the upstream turbine is operating at design conditions throughout this study. However, it should be mentioned that as the upstream turbine operates in yaw, this might change the optimal operation. Different yaw angles of $\gamma = 0^\circ, 10^\circ, 20^\circ, 30^\circ, 40^\circ$ and 50° were examined in terms of how they were affecting the power and thrust coefficient. Yawing the turbine will affect both the power and thrust coefficient significantly. By yawing the turbine, the angle of attack will change, and so will the aerodynamic behavior on the rotor blades.

The power deficit at increasing yaw angles is illustrated in Figure 6.2. The graph clearly shows that the efficiency decreases significantly with increasing yaw angles, which is due to the area swept by the rotor has been reduced, thus less power is extracted from the air flow, as further described in section 3.3. In addition to the power loss, the run-away point where the wind turbine no longer extracts energy from the wind appear at a lower tip speed ratio in yawed operation. From the C_p -curve presented previously for un-yawed conditions, the run-away point is seen to appear at $\lambda = 11.1$. The same pattern can be seen for the thrust coefficient, in Figure 6.3. The thrust coefficient decreases with increasing yaw angle for the same reasons as the power coefficient decreases. The power output of a turbine operating at a certain yaw angle is estimated to fall with $C_p(\gamma) = C_p(\gamma = 0)\cos^3(\gamma)$. [20] This rough calculation may be useful as a control parameter in terms of yawing certain turbines to increase the total power output of a wind farm. The cosine function is also plotted together with the actual power coefficient.

The power curve fits the approximation very well, as seen in Figure 6.2. For this reason, it seems to be a decent control parameter for this study.

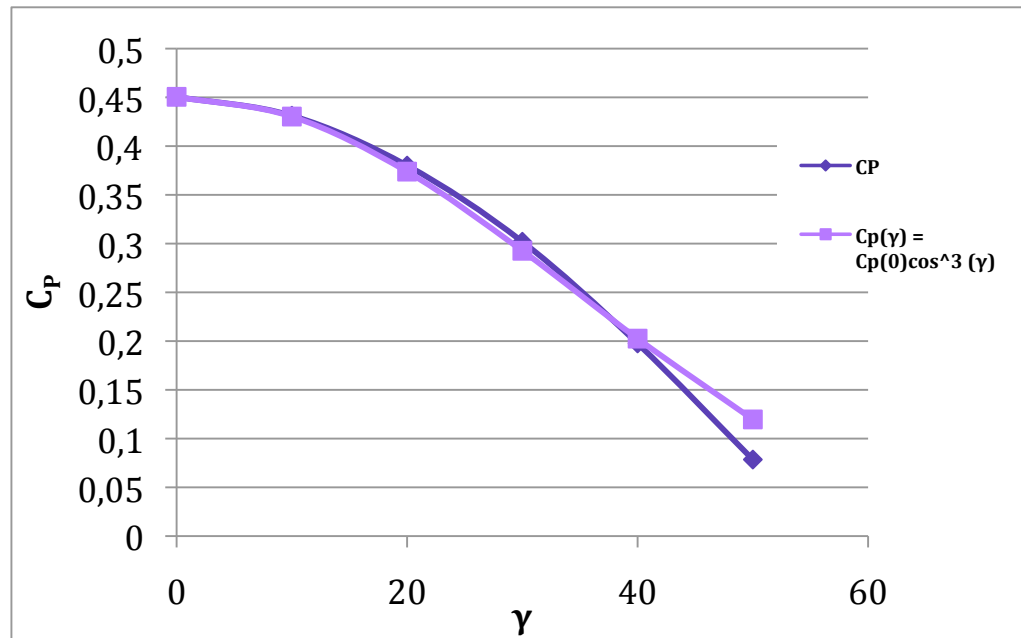


Figure 6.2 – Power coefficient for the model turbine at $\lambda = 6$ while varying yaw angles, γ .

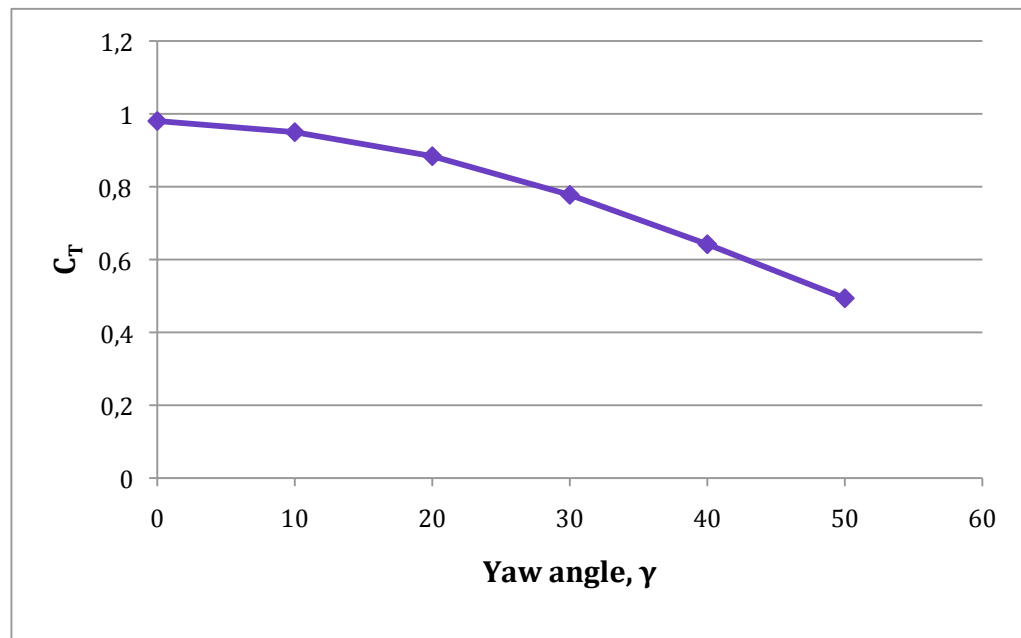


Figure 6.3 – Thrust coefficient for the model turbine at $\lambda = 6$ while varying yaw angles, γ .

6.1.2 Downstream flow field

The downstream flow field of the upstream turbine operating at different yaw angles was inspected in terms of mean velocities and turbulence intensities.

Horizontal velocity profiles

In order to fully utilize the potential of using yaw as an active control, it is necessary to have good knowledge of the horizontal velocity profiles downstream. To get a better understanding of what happens to the wake behind a yawed turbine, the mean velocity profiles were determined using a pitot probe at several different positions downstream while varying the yaw angle of the upstream turbine. The resulting velocity profiles with yaw angles of 0°, 20° and 40° are presented in Figure 6.4, Figure 6.5 and Figure 6.6, respectively. The distances are non-dimensionalized by the rotor radius and the velocities are normalized with the reference velocity. Consequently, the velocity profiles represent the velocity deficit rather than the actual velocity. Zero on the x-axis represents the center of the rotor, and the area from $z/R = -1$ to $z/R = +1$ represents the width of the rotor area (diameter). As expected, there is a greater velocity deficit behind the rotor area, since this is where the wake takes place.

Starting with the case for when the upstream turbine is operating in un-yawed conditions, see Figure 6.4, the horizontal velocity profiles can be characterized as axis-symmetrical. The velocity deficit seen behind the rotor area has a natural cause, as the wind is “used” it will be lower, consisting of a greater amount of turbulence. At 1D, the velocity deficit is observed to be greater behind the rotor blades than behind the nacelle area, which is due to the spinning blades creating a greater force slowing down the wind compared to the force created by the nacelle and tower. By analyzing the development of the mean velocities, it can be observed that the velocity deficit due to the presence of the nacelle and tower recovers gradually further downstream. At 4.78D downstream, the velocity deficit behind the nacelle and rotor is barely noticeable. It can also be seen that the velocity deficit becomes broader downstream, which is especially noticeable at 4.78D, and is a result of the shear layer’s growth when moving downstream, due to the mixing with the surrounding flow as explained in section 3.1. Furthermore, moving downstream, the velocity curves become smoother with less high velocity variations, as a result of the free stream mixing with the turbulent flow inside the wake.

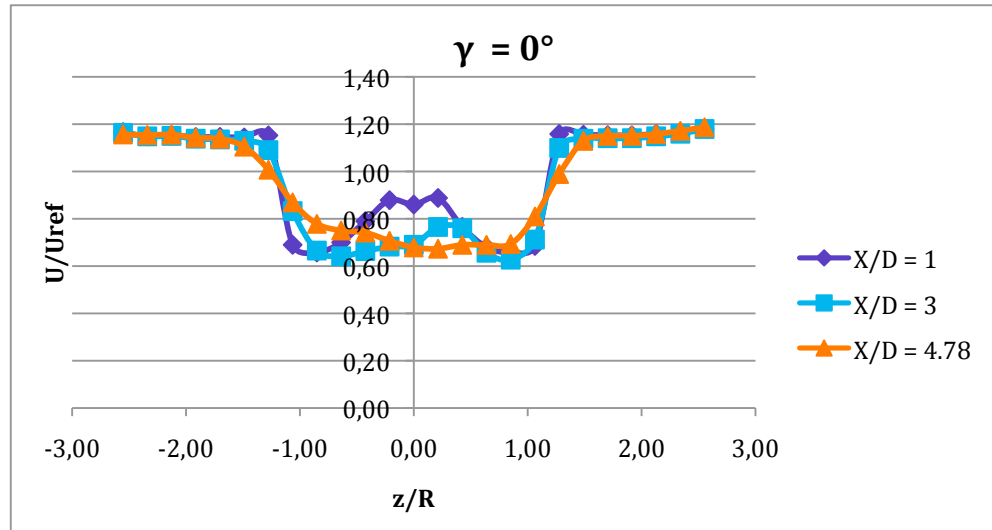


Figure 6.4 – Horizontal velocity profile with zero yaw

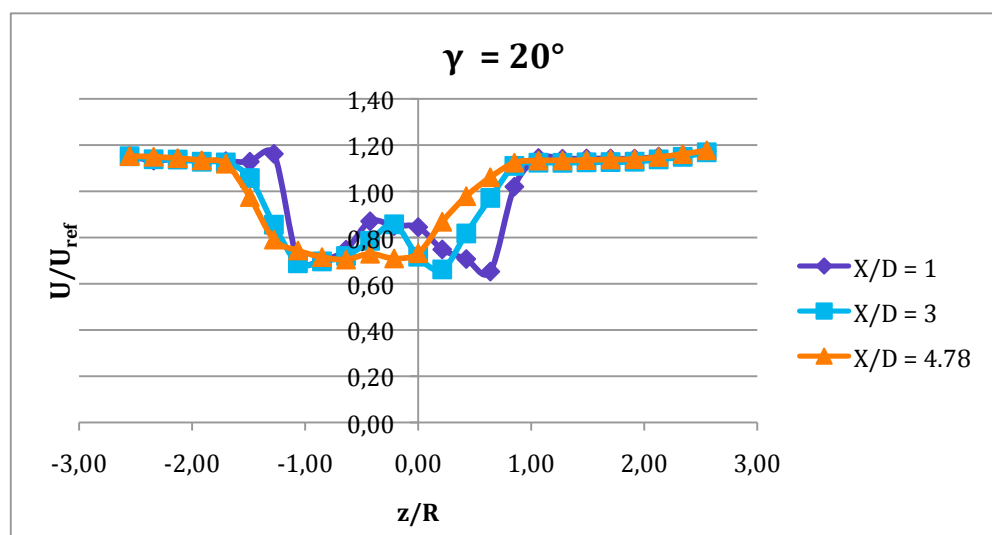


Figure 6.5 – Horizontal velocity profile with $\gamma = 20^\circ$

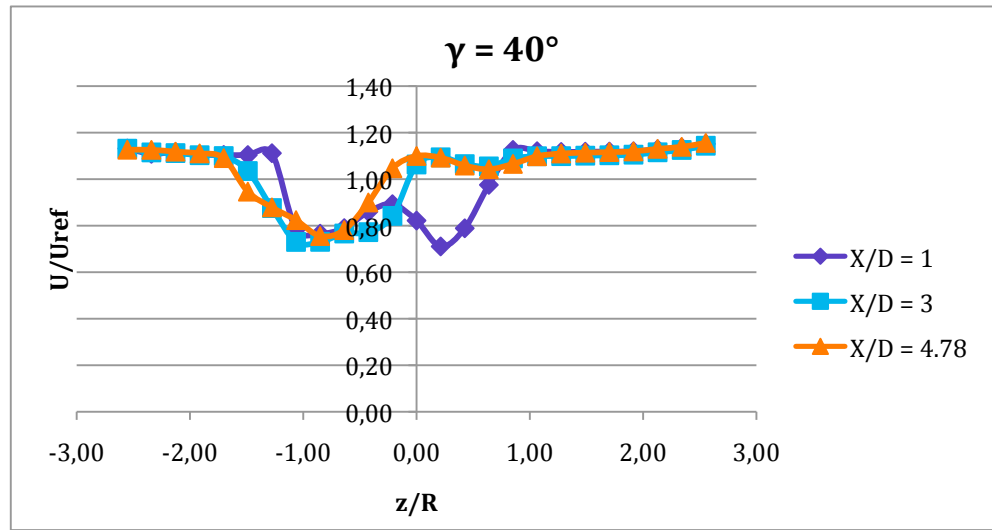


Figure 6.6 – Horizontal velocity profile with $\gamma = 40^\circ$

In the outer region of each velocity profile there is a systematic excess velocity relative to the free stream velocity, of approximately 11-15%, depending on the turbine's degree of yaw. As the rotor is spinning, it appears as a flat disk blocking the wind to a certain extent and the wind will therefore flow around the blockage. As a result of this combined with the wall interference, the velocity will increase. The blockage ratio for the model turbine used in the specific wind tunnel operating in un-yawed conditions is about 12.8%, which correspond to the velocity increase above the free stream velocity of 11-15%. The correlation between these two factors can be explained using the continuity equation, $\rho_1 A_1 U_{ref} = \rho_2 A_2 U_2$, where $\rho_1 = \rho_2$. When the airflow reaches the rotor, the cross-sectional area, A, is decreasing because of the rotor and tunnel walls are blocking the wind, hence the velocity, U, is increasing. The velocity increase is given by

$$U_2 = \frac{U_{ref} A_{tunnel}}{A_{tunnel} - A_{rotor}} \quad (6.1)$$

where the cross-sectional area of the tunnel is $A_{tunnel} = 2m \times 2.7m$, and the rotor swept area for the un-yawed rotor is $A_{rotor} = \pi \times 0.47^2$. The resulting velocity increase from this is given as $U_2 = 1.146 \times U_{ref}$, which supports the prior statement of an excess of about 15% of the reference velocity at the most. Yawing the turbine deceases the rotor swept area, thus there is a reduction in the blockage ratio, which results in a lower velocity excess of the reference velocity. In this case, the velocity exceeds the free stream velocity of about 11% when the turbine is yawed 40° .

Since the tip speed ratio is not higher than 6, the rotor area does not appear as that strong of a blockage, hence only a part of the flow will go around the rotor, resulting in a less dramatic velocity increase. In addition, neither of the velocity profiles shows any velocity drop close to the walls, which confirms that none of the velocity measurements were disrupted by the boundary layer.

For the next two scenarios with $\gamma=20^\circ$ and $\gamma=40^\circ$, the wakes are no longer axis-symmetric as seen in Figure 6.5 and Figure 6.6, and the effect of yawing is obvious.

It is clearly visible that the wakes are now deformed and deflected towards the LHS, as a response to the side force acting on the turbine in the positive z-direction.

When the upstream turbine is yawed, the wake will be compressed, and at the same time deflected to the side. This is especially noticeable for $\gamma=40^\circ$, where the width of the wake is about half of what it is with zero yaw and at the same time shifted approximately 0.5D

towards the LHS at $x/D = 3$, and even further to the left downstream. Hence, it may be observed that as the yaw angle increases, so does the skew angle of the wake. Also, as explained in the theory section, the skewed wake has the downwind part of the rotor (LHS) closer to the wake centerline than the upwind part of the rotor, which can be confirmed by these velocity profiles.

It seems to be a significant gain in deflection by going from a yaw angle of 20° to a yaw angle of 40° . Yawing the turbine 40° , the wake is more or less fully deflected away from the center of the tunnel at both $x/D = 3$ and $x/D = 4.78$. If a turbine were to be placed at these positions, it would only be partly exposed to the wake, thus the rotor sweeps a smaller part of the turbulent airflow. This will be examined further in this report.

Horizontal turbulence intensity profiles

A good knowledge of the horizontal velocity profiles downstream has been obtained from the above measurements using a pitot probe. In this section, measurements of the horizontal velocity profile located 3D downstream of the yawed upstream turbine were carried out using a hot-wire probe, to get a more detailed understanding of the phenomena involved. As information on the horizontal velocity profile 3D downstream was already known, it was possible to predict the approximate locations where the turbulence level would peak. In addition to the turbulence intensity, mean velocities were also obtained from the hot-wire measurements. The mean velocities acquired 3D downstream match very well with the previous results from the pitot probe and ensure the fact that the data is reliable. The comparison of the mean velocity profiles at $x/D = 3$ with a pitot probe and a hot-wire probe can be seen in Appendix B.1.

Figure 5.7 – 5.9 show the non-dimensional cross-sectional distribution of turbulence intensity, u'^2/U_{ref}^2 , when the upstream turbine is operating at varying yaw angles.

In the near wake ($x/D = 3$) for all yaw angles, considerably large peaks in the turbulence intensity are seen to appear around the tip of the turbine wake. This is associated with the high turbulence levels produced by the helicoidal vortex that originate from the tip-vortices of the three turbine blades. From Susanne Lynum's Master's Thesis "Wind turbine wake meandering" carried out for the same model turbine as for this present study, it is proven that the three tip vortices do not follow the same path for un-yawed conditions, meaning they are not completely in line. However, the distances keeping them from being in a perfect line are quite small. As the pitch angles are set and measured by hand, it is nearly impossible to set a pitch angle perfectly to zero, and a minimal error between the tip vortices' paths will occur.

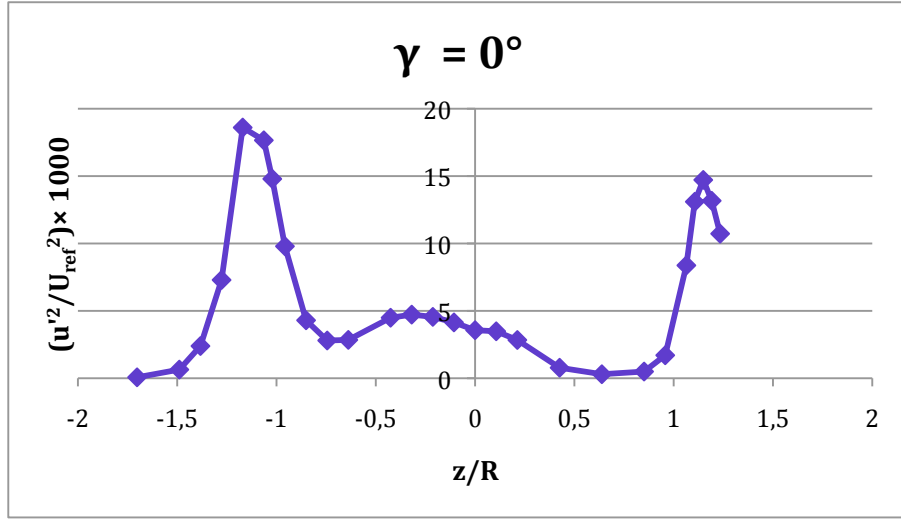


Figure 6.7 – Horizontal turbulence intensity profile at $x/D = 3$ downstream of the upstream turbine at zero yaw.

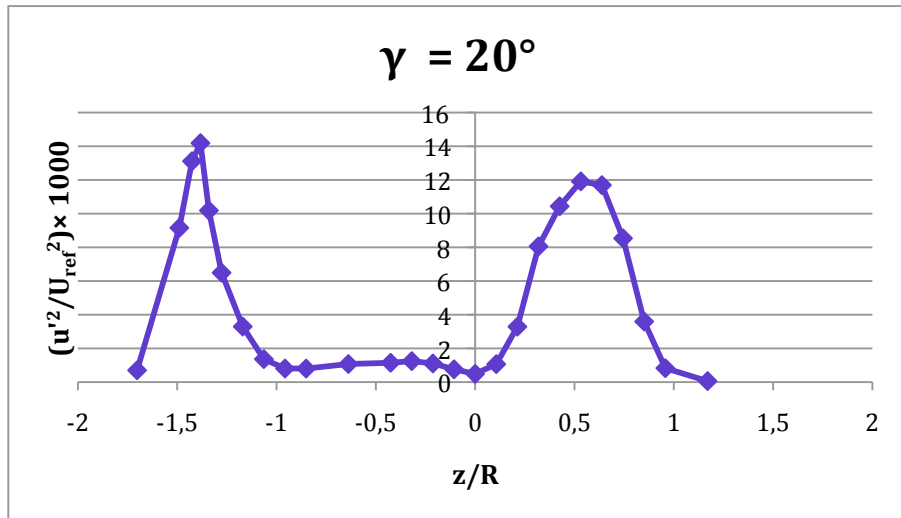


Figure 6.8 – Horizontal turbulence intensity profile at $x/D = 3$ downstream of the upstream turbine yawed 20° .

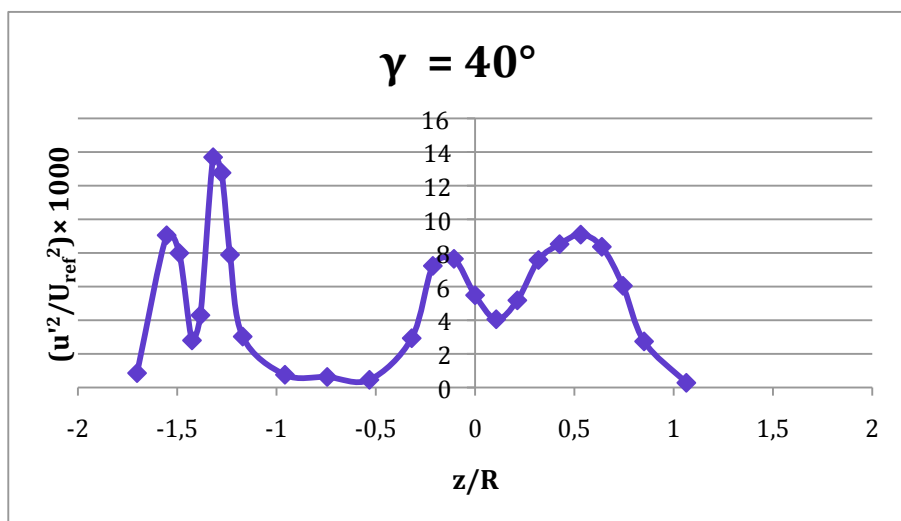


Figure 6.9 – Horizontal turbulence intensity profile at $x/D = 3$ downstream of the upstream turbine yawed 40° .

From analyzing the un-yawed case (see Figure 6.7) it can be seen that there is one maxima in the shear layer on each side of the wake. For this reason, the tip-vortices seem to have merged and paired into groups. If the tip vortices were to follow the same path perfectly, the turbulence intensity peaks would have appeared stronger including a steeper and narrower peak. The interior of the wake is observed to consist of a much lower and broader amount of turbulence, which can be traced back to a combination of the presence of the tower, as well as the root vortices. Further, the turbulence intensity is observed to be greater on the LHS of the rotor. Due to the counter-clockwise rotating turbine, a clockwise rotating flow is induced in the wake, as explained in section 3.1. As a result of this, the rotating flow will hit the upper part of the tower at a certain angle, causing the flow to deflect a little to the LHS of the rotor. [27] This phenomena is clearly seen in the turbulence intensity distribution of the 3D wake, and corresponds to the asymmetrical velocity deficit of the 3D wake in Figure 6.4 for zero yaw. As it may be observed, the wake is still after 3D affected by the rotor and the nacelle to a small extent, which can also be confirmed by the mean velocity profiles presented.

For the two cases when the upstream turbine is operating in yaw, the turbulence intensity profiles are found to be less axis-symmetric, see Figure 6.8 and Figure 6.9. With increasing yaw angle, the turbulence intensity peaks become narrower on the LHS, and wider on the RHS. This may be intrigued by the existence of the wall on the left side, interfering with the flow. As the skewed wake is compressed and deflected to the LHS of the rotor, the wake is most likely further compressed due to the presence of the wall. On the RHS of the rotor, the wake can expand more freely, thus the turbulence intensities appear on a wider area. Another effect that may lead to an even wider turbulence area associated with the tip vortices is the turbulence created from the tower. When the yaw angle is increasing, the tip vortices will arise closer to the center of the rotor and also closer to the tower. This may lead the tip vortices to expand due to the turbulence air produced at the tower.

A remarkable change can be seen when yawing the upstream turbine from $\gamma=20^\circ$ to $\gamma=40^\circ$, where the two turbulence peaks are turned into four significant peaks. Without further detailed data the reason for this phenomena cannot be confirmed, although it is a very interesting occurrence. The only realistic explanation that comes to mind is that it may seem like the tip vortices are separated. It may look like it can exist two tip vortices in the two higher peaks on each side of the rotor, and one tip vortex in each of the two lower peaks. As mentioned previously, the tip vortices do not follow the same path. As the yaw angle increases, it may look like this induces a further increase in the relative distance between the tip vortices.

From Figure 6.9, it seems like the relative position between one of the tip vortices has increased more than the relative position between the two other tip vortices, where this indication originates from observing two turbulence peaks in the shear layers instead of one. However, this cannot be confirmed and is only an indication on what may have caused the turbulence peaks to part. By doing a smoke visualization in the wind tunnel it is possible to visualize the vortices and understand more of what is happening to the tip vortices with increasing yaw angle.

6.2 Wake interference on a second (downstream) model turbine

A second (downstream) turbine was mounted at $x/D = 3$ downstream of the first (upstream) turbine, and the influence of the wake of the upstream turbine onto the performance and dynamic behavior of the downstream turbine were studied.

6.2.1 Performance

The performance characteristics of the present model turbine in an unobstructed environment are the same as for the upstream turbine, as presented earlier. Its maximum power coefficient is therefore $C_p = 45.6\%$ when operating at design conditions ($\lambda=6$). Figure 6.10 shows how an upstream turbine operating under varying yawed conditions affects the performance of the downstream turbine.

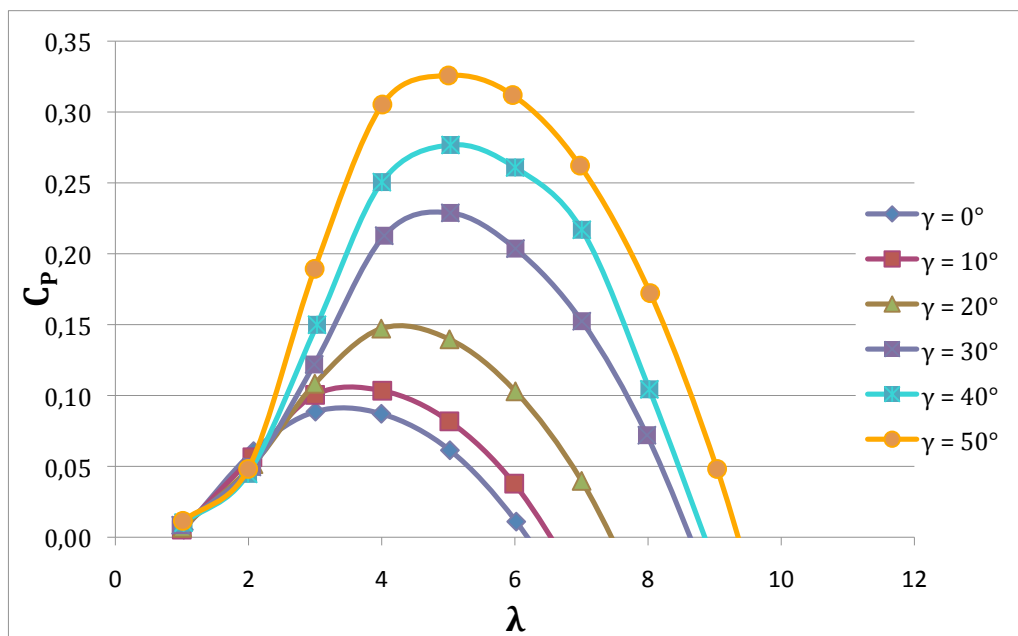


Figure 6.10 – The performance of the second (downstream) turbine at $x/D = 3$ when the first (upstream) turbine operating at different yaw angles at design condition.

As the yaw angle of the upstream turbine increases, there is a continuing increase in the power coefficient of the downstream turbine, except for very low tip speed ratios, where the operation occurs within the stall region. There are two effects leading to the increased efficiency for the second turbine when the upstream turbine is operating under yawed conditions. As the upstream turbine is operating under yawed condition, the area swept by the rotor is reduced and the upstream turbine extracts less power. This leaves more potential in the wind for the second turbine to capture. The other effect this has on the performance of the downstream turbine is that the wake is deflected sideways, thus the downstream turbine

is only partly exposed to the wake and thereby experiences less interaction with the wake. In addition to improved performance, it is observed that the range of the operating tip speed ratio is also increased as the turbine is less affected by the wake. The cut-in wind speed for the downstream turbine is therefore reduced, and the turbine can start producing power at lower wind speeds, due to the higher tip speed ratios seen in Figure 6.10.

The maximum power coefficient of the second turbine for each corresponding yaw angle is presented in Figure 6.11. The graph shows a significant increase in the maximum power coefficient when further increasing the yaw angle from 10° . The greatest increase takes place when yawing the turbine from 20° to 30° , obtaining a power coefficient of 23%. At a yaw angle of $\gamma = 10^\circ$, the gain is only about 1% compared to when the upstream turbine is operating at zero yaw. However, at a yaw angle of $\gamma = 50^\circ$, the gain is about 24% compared to the un-yawed condition. This clearly demonstrates the great improvement of the efficiency of the downstream turbine when applying yaw as an active power control. This being said, the gain in the downstream turbine's power output may not necessarily increase the overall power output for the two turbines, as the upstream turbine will experience a decrease in the power output with increasing yaw angles.

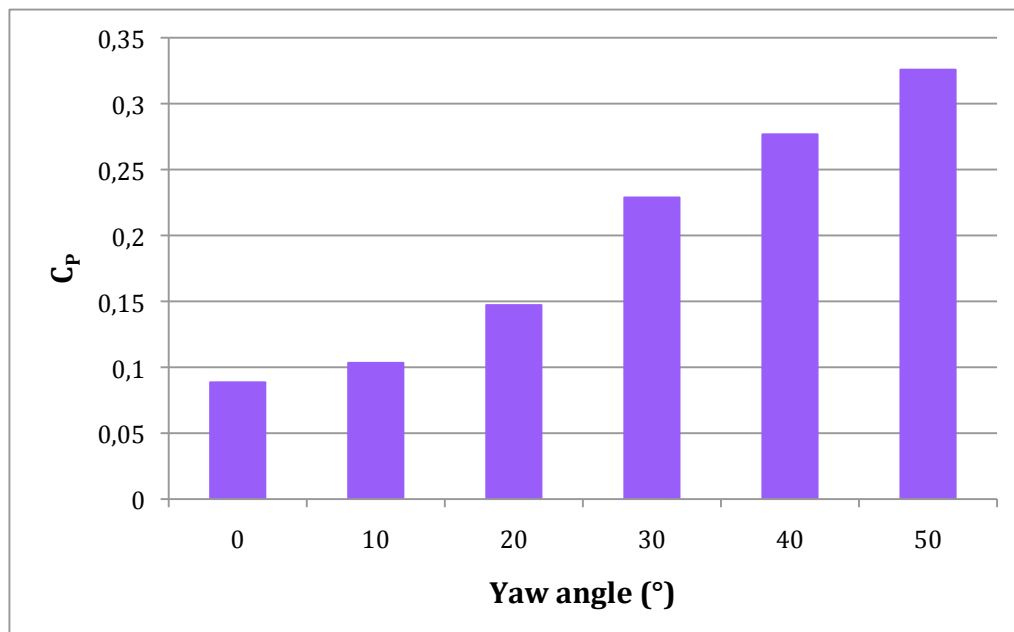


Figure 6.11 – The maximum power coefficient of the second (downstream) turbine at $x/D = 3$ with the first (upstream) turbine operating at different yaw angles.

In addition to yawing the upstream turbine, it may be possible to further increase the power coefficient by pitching the blades of the downstream turbine, but this is not experimented on in the present study.

6.2.2 Dynamic loads

The dynamic loads (torque) experienced by the rotor blades of the downstream turbine while the upstream turbine is operating at varying yaw angles are presented in Figure 6.12.

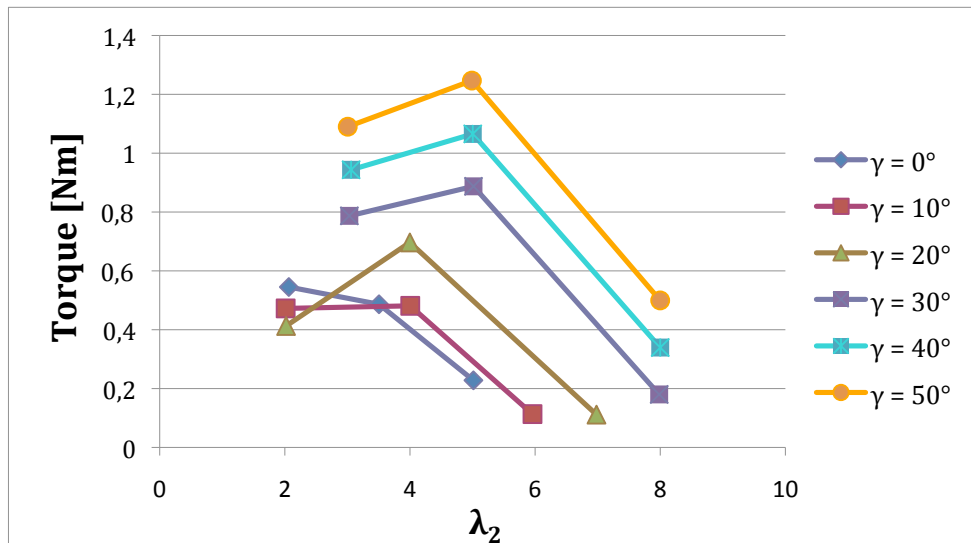


Figure 6.12 – Mean torque experienced by the downstream turbine operating at different tip speed ratios, while the upstream turbine is operating in various yawed conditions.

It can be observed that the mean torque on the downstream turbine increases with increasing yaw angle of the upstream turbine. When the yaw angle increases, the skew angle of the wake will also increase, and the second turbine's interference with the wake is reduced. The turbine is only partly exposed to the wake and therefore it experiences higher wind velocities, resulting in higher performance, thus higher torques are produced. This is also shown in the previous section, where its performance increases with increasing yaw angle of the upstream turbine.

Although the average torque will increase, the turbine blades will experience varying torques depending on where they are in their path. When the downstream turbine is partly exposed to the wake, the blades will move partially in and out of the turbulent wake during each rotation of 360° causing high variations in torque. The fluctuations in torque will result in non-symmetrical loads acting on the turbine. For this reason, the standard deviation of the torque experienced by the blades is as important as the average torques when studying the dynamic loads.

The standard deviation of the torques produced can be seen in Figure 6.13 below.

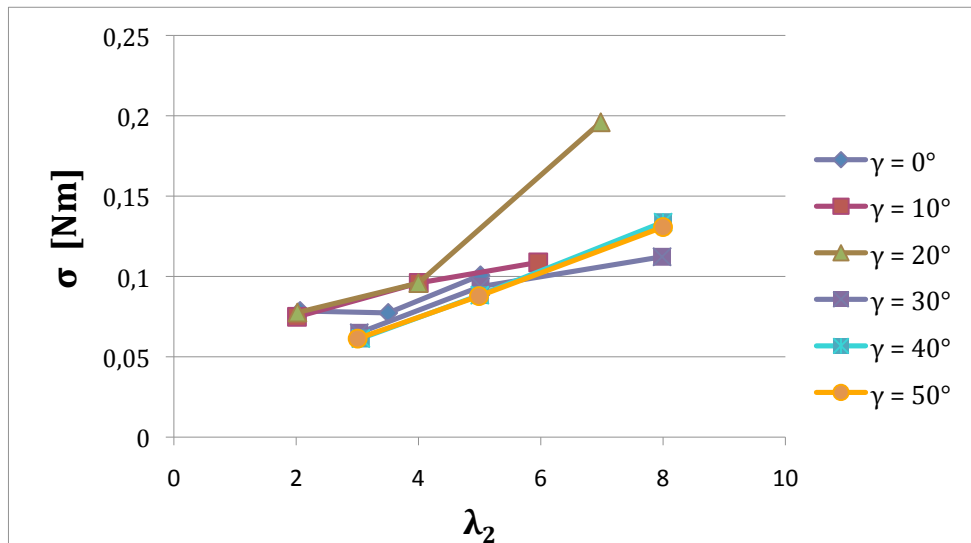


Figure 6.13 – Standard deviation of the torque experienced by the downstream turbine operating at different tip speed ratios, while the upstream turbine is operating in various yawed conditions

First of all, it is observed that all curves follow the same pattern, except for the point with $\lambda_2 = 7$ and $\gamma = 20^\circ$. Because this single point deviates significantly from the systematic pattern, it may be safe to say that something has disrupted the specific measuring point, and it will therefore be neglected when further discussing the results. By further analyzing, the standard deviation curves seem to be more or less constant for different yaw angles, and are mostly depending on the rotational speed of the downstream turbine. The standard deviation of the torque does not seem to increase with increasing yaw angles and is approximatley constant for each yaw angle, which is highly unexpected. There is no good explanation for why the results deviate from the theory, except the possibility of noise disturbing the torque signals. During the experiment, eccentricity was observed in the shaft which may induce higher loads. Due to witnessing the unbalance in the turbine, it is reasonable to believe that the signals are affected by this unbalance. A possible explanation may therefore be that the resulting signals consists of a combination of dynamic loads acting on the blades and dynamic loads caused by the eccentricity in the shaft. As the rotational speed increases, so will the loads induced by the unbalance in the turbine. The respective impact from the actual loads acting on the blades and the loads induced by the unbalance is unknown, which makes it difficult to conclude on the torque fluctuations experienced by the blades. However, the noise added on the sinusoidal signal will not affect the mean values, which seems to have provided reliable results during the present study based on theoretical aspects and expectations.

6.3 Wind farm efficiency

In this section the overall power output from the two turbines are compared for different combinations of operation. The wind farm efficiency is defined as

$$\eta = \frac{P_1 + P_2}{\frac{1}{2} \rho A U_{ref}^3} = C_{p1} + C_{p2} \quad (6.2)$$

where P_1 and P_2 represent the power produced by the first (upstream) turbine and the second (downstream) turbine, respectively. Figure 6.14 shows the overall efficiency of the two turbines, as well as each turbines power contribution for the different yaw angle conditions. As expected, the decrease in the power contribution from the upstream turbine results in a significant increase in the power contribution from the downstream turbine.

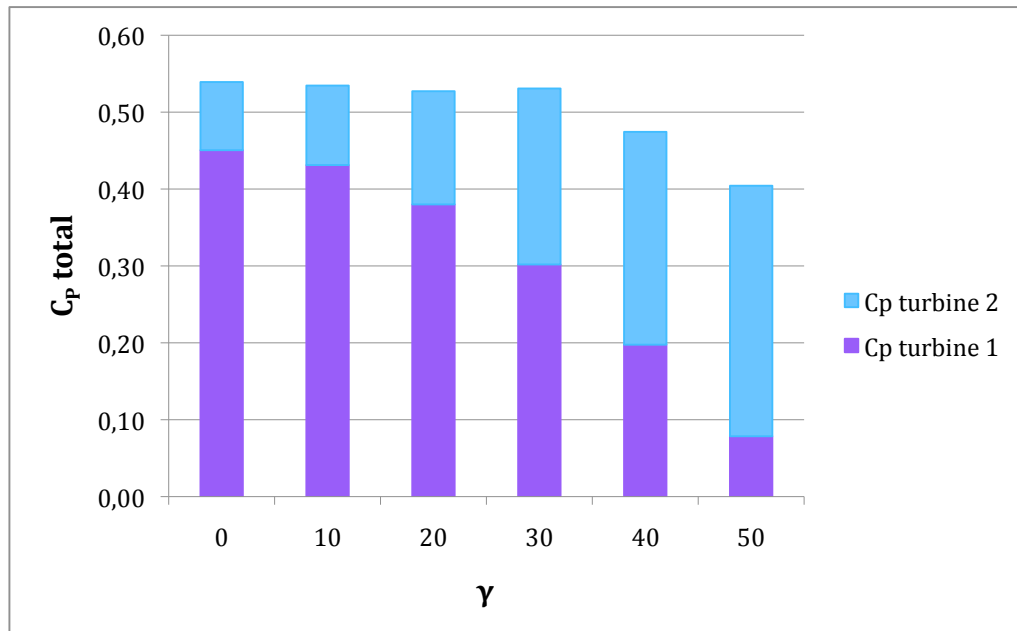


Figure 6.14 – Wind farm efficiency of the two turbines, where the downstream turbine is operating at maximum power coefficient at $x/D = 3$ when the upstream turbine is operating at varying yaw angles.

The greatest wind farm efficiency is seen to occur in the region of yawing the upstream turbine from 0° to 30° , where the efficiency is more or less constant for each case, at approximately 53-54%. The power loss experienced by the upstream turbine is within this region balanced with the corresponding power gain of the downstream turbine. When the upstream turbine is yawed more than 30° , the power losses of yawing the turbine is greater than the gain in the downstream turbine, and therefore not very advantageous. This was more or less expected, as yaw angles of 40° and 50° are relatively large angles, thus a dramatic

power decrease will occur for the yawed turbine. Yawing a turbine to that large extent is not widely applied, and it can be confirmed in this study that it is not particularly beneficial. When the upstream turbine is operating at its maximum yaw angle ($\gamma = 50$) the power coefficient of the downstream turbine is about 33%. This means that the upstream turbine is still affected by the wake, as it has not reached its maximum power coefficient of 45.6%. The mean velocity profiles presented previously is measured up to $\gamma=40^\circ$, where it can be seen that the wake at 3D downstream is deflected away from the center of the rotor, thus only the left side of the rotor is exposed to the wake. This seems to correspond with the power coefficient of 33% at $\gamma=50^\circ$, as the wake cannot deflect as much as one radius further to the left by only increasing the yaw angle by 10° .

7 Conclusion

The study confirms that when a turbine is operating in yaw, both the power coefficient and the thrust coefficient will be affected due to the change in aerodynamic behavior on the rotor blades. The power and thrust coefficient will decrease significantly with increasing yaw angle. The decrease in the power coefficient is estimated to fall with $C_p(\gamma) = C_p(\gamma = 0)\cos^3(\gamma)$, which is proven to be a decent control parameter when designing a wind farm in this study.

The effect of yaw on the downstream flow field is clear, where the wake is deformed and deflected to the left side, due to the side force acting on the turbine. When yawing the turbine 40° the width of the wake at 3D downstream is decreased to half its size of un-yawed condition and is shifted approximately 0.5D towards the LHS of the rotor, and even further downstream. The skew angle is increasing with increasing yaw angle, as expected.

The peak turbulence intensities occur in the shear layer, also corresponding to the area consisting of the greatest mean velocity deficits. As the yaw angle increases, the turbulence intensity region associated with the shear layer becomes narrower on the left side, where the wake is deflected, and the wall blockage effect due to the wall is visible. On the RHS, the shear layer is expanding more freely combined with turbulent air from the tower interfering with the tip vortices, causing the turbulence intensities to appear on a wider area.

The second turbine mounted 3D downstream has a continuing increase in power with increasing yaw angle of the upstream turbine. This confirms that as the upstream turbine is yawed, the downstream turbine experiences less interaction with the upstream turbine. When the upstream turbine is yawed 50° , the downstream turbine obtain a power gain of 24% compared to the un-yawed condition, resulting in a maximum power coefficient of 33%. The greatest relative gain in power takes place when yawing the turbine from 20° to 30° , obtaining a power coefficient of 23%. This clearly demonstrates a great improvement of the efficiency of the downstream turbine when applying yaw as an active power control.

The optimal wind farm efficiency occurs when the upstream turbine is yawed between 0° to 30° , resulting in a wind farm efficiency of approximately 54% for all three conditions. The power loss experienced by the upstream turbine is outweighed with the corresponding power gain of the downstream turbine. However, when a wind turbine is yawed, it will experience fluctuation in blade loads, and such fluctuations will cause fatigue loads reducing its longevity. As the downstream turbine is partly exposed to the wake, it will also experience non-

symmetrical loads and affect its longevity. The result of the analysis suggests that unless the wake from the upstream turbine is fully deflected away from the downstream turbine, the asymmetrical loads will cause more damage than larger, average induced loads that are symmetrical.

Therefore, the conclusion of this study carried out on two wind turbines in the wind tunnel is that it will not be beneficial to use yaw as a mechanism for controlling the wake direction and thereby increase the wind farm efficiency since the power gain of the downstream turbine will be offset by the power loss of the yawed turbine. However, if it is known that yaw is to be employed frequently on certain turbines in a wind farm, tailored blade design may have a positive impact on the overall wind farm efficiency and also reduce fatigue loads. Such blade design would prevent sections of the blade from moving in and out of stall, thus fluctuating loads are reduced and power output is maximized.

8 Further work

The operation of wind turbines in yaw represents a special case of aerodynamic behavior that is not yet fully understood, and needs to be studied more thoroughly. It certainly affects the performance as well as the turbine design. For this reason, more experiments should be done in terms of analyzing the wake behavior downstream, and also the asymmetrical loads that are experienced by both the yawed turbine and downstream turbines.

When it comes to the overall efficiency of a wind farm in future testing, there are further measurements that can be conducted in addition to what has been done in this report. In this report, the yawed upstream turbine was operating at fixed rotational speed, which will affect the operation of the downstream turbine. It may be interesting to see how varying the rotational speed of the upstream turbine will affect the overall efficiency when it is operating in yaw. Also, a downstream turbine was placed 3D downstream in the present report where the best operating points resulted in an equal gain in power as the power losses experienced by the yawed turbine. It may be interesting to place a downstream turbine farther downstream (at 5D) to measure its performance, since the wake is more deflected away from the centerline at this location. Finally, the overall efficiency may be increased by combining an upstream turbine in yaw together with a downstream turbine operating with different pitch angles.

The results of the measurements of the dynamic loads experienced by the downstream turbine partly exposed by the wake raised more questions than answers. As the standard deviations were not in accordance with the expectations, further experiments should be conducted.

Further tests should also be undertaken in order to determine the wake behavior of a yawed wind turbine. The experimental results revealed an interesting occurrence of the turbulence intensities when the upstream turbine was yawed 40° . These effects have been discussed in this report, and there are indications that they may be caused by tip vortices grouping in pairs of two. A closer look at what is happening can be further explored using smoke visualization in the wind tunnel. In general, there are few experiments performed on skewed wakes, and particularly in terms of turbulence intensities.

9 Bibliography

- [1] J.F. Manwell, J.G. McGowan, and A.L. Rogers, *Wind Energy Explained*, 2nd ed. PO19 8SQ, West Sussex, United Kingdom: John Wiley and Sons Ltd., 2009.
- [2] Wikipedia. [Online]. http://en.wikipedia.org/wiki/Betz'_law
- [3] Gurit. (2013) Wind Energy Handbook. [Online].
http://www.gurit.com/files/documents/2_aerodynamics.pdf
- [4] Danish Wind Industry Association. Power Control. [Online]. <http://wiki.windpower.org>
- [5] Davide Medici, "Wind Turbine Wakes - Control and Vortex Shedding," KTH Royal Institute of Technology, Stockholm, Technical report Mars 2004. [Online].
http://www.elforsk.se/Global/Vindforsk/Rapporter_fran_aldre_program/Medici_2004_Wakes.pdf
- [6] Bindi Chen. (2013, Jan) Pitch-regulated and Stall-regulated Wind Turbine. [Online].
www.bindichen.co.uk
- [7] Magdi Ragheb and Adam M. Ragheb, "Wind turbines theory - The betz equation and optimal rotor tip speed ratio," University of Illinois at Urbana Champaign, USA, Scholar work 978-953-307-508-2, 2011.
- [8] B. Sanderse, "Aerodynamics of Wind Turbine Wakes," ECN, literature review 2009.
- [9] J.F. Ainslie, "Calculating the field in the wake of wind turbines," in *Journal of Wind Engineering and Industrial Aerodynamics*, 27:213-224., 1988.
- [10] Frank M. White, *Fluid Mechanics*, 6th ed., The McGraw-Hill Companies, Ed. 10020, NY, USA: McGraw-Hill, 2008.
- [11] F.M. White, *Viscous Fluid Flow*, 2nd ed.: McGraw-Hill, 1991.
- [12] Wikipedia. (2013, May) Turbulence kinetic energy. [Online]. <http://www.wikipedia.org>
- [13] National Oceanic and Atmospheric Administration. (2011, April) NOAA. [Online].
http://www.noaanews.noaa.gov/stories2011/20110426_windwakes.html
- [14] Kimberly E. Diamond and Ellen J. Crivella, "Wind Turbine Wakes, Wake Effect Impact and Wind Leases: Using Solar Access Laws as the Model for Capitalizing on Wind Rights During the Evolution of Wind Policy Standards," 2011.
- [15] ENOVA SF, "Potensialstudie Havenergi," 2007.
- [16] Kari Melby Loland, "Wind Turbine in Yawed Operation," Department of Energy and Process Engineering, Norwegian University of Science and Technology, Trondheim, Master's Thesis 2011.
- [17] Erich Hau, *Wind Turbines - Fundamentals, Technologies, Application, Economics*, 2nd ed.: Springer, 2006.
- [18] Tony Burten, Nick Jenkins, David Sharpe, and Ervin Bossanyi, *Wind Energy Handbook*, 2nd ed.: John Wiley and Sons, Ltd., 2011.
- [19] M. S Adaramola and P.-Å. Krogstad, "Experimental investigation of wake effects on wind turbine performance," Norwegian University of Science and Technology, 2011.
- [20] P.-Å Krogstad and J.A. Karlsen, "An experimental and numerical study of the performance of a model turbine,".
- [21] L.J. Vermeer, N. J. Sørensen, and A. Crespo, "Wind turbine wake aerodynamics," Progress in Aerospace Sciences, 2003.
- [22] Otto De Vries, "On the theory of the horizontal-axis wind turbine," Ann Rev Fluid Mech, 1983.
- [23] Tom Lecklider. (2007, June) 200 MPH is a breeze. [Online].
<http://www.evaluationengineering.com/articles/200706/200-mph-is-a-breeze.php>
- [24] Tom Benson. (2010, August) Pitot-static tube. [Online]. <http://www.grc.nasa.gov/WWW/k-12/airplane/pitot.html>
- [25] D. Olvari and M. Carbonaro, "Chapter 5 Hot-wire measurements," in *Measurement Techniques in*

Fluid Dynamics, 2nd ed., Theodore von Karman, Ed.: Institute for Fluid Dynamics, 2004, pp. 195-228.

- [26] Wikipedia. Wikipedia: Anemometer. [Online]. <http://en.wikipedia.org/wiki/anemometer>
- [27] Jan Bartl, "Wake measurements behind an array of two model wind turbines," Division of Heat and Power Technology , KTH School of Industrial Engineering and Management , 100 44, Master of Science Thesis 2011.
- [28] Birgitte Andresen, "Interactions between two wind turbines," Department of Energy and Process Engineering, NTNU, 70, Project Thesis 2012.

APPENDIX A Calibration

Calibrations were conducted several times for each instrument, as the measurements were done at different times, either days or weeks apart. Since the calibration constants achieved for each instrument are very similar, and the procedure is the same, only one calibration curve for each instrument is shown.

A. 1 Torque

The calibration curve for the torque is given by:

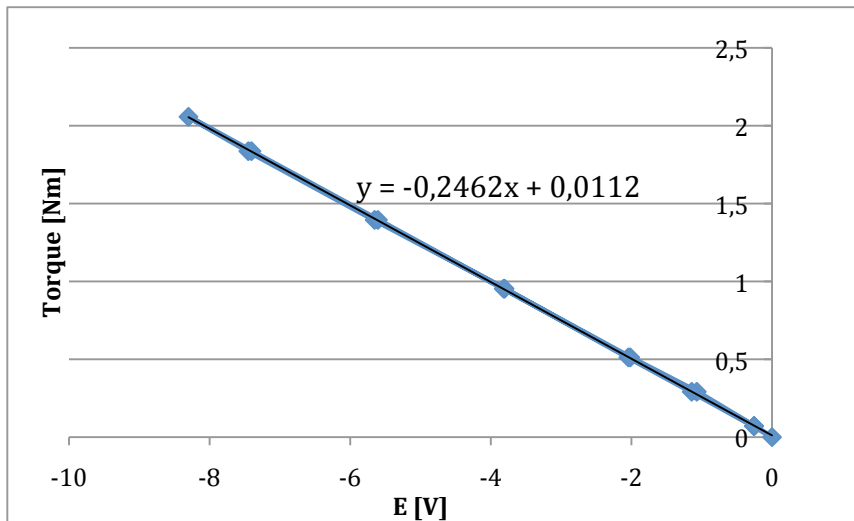


Figure A. 1 – Calibration curve, torque.

From the calibration curve, the torque is given by:

$$F_T = (-0.2462) \times dE_Torque \quad [\text{Nm}] \quad (\text{A.1})$$

Where F_T is the torque, and E represents the voltage signal.

The off-set voltage was 8.82797 V with an amplifier gain of 2. The data used to plot the calibration curve are shown in table A.1.

Table A. 1 – Calibration data, torque.

Temp[C°]	E_Torque [V]	dE_Torque[V]	Mass [g]	Torque[Nm]
22,47613	8,82797	0	0	0
22,39561	8,57374	-0,25423	16	0,070632
22,3314	7,75856	-1,06941	66	0,291357
22,40497	6,81177	-2,0162	116	0,512082
22,41133	5,01076	-3,81721	216	0,953532
22,3941	3,22236	-5,60561	316	1,394982
22,32818	1,42361	-7,40436	416	1,836432
22,31383	0,52724	-8,30073	466	2,057157
22,19547	1,37831	-7,44966	416	1,836432
22,30136	3,17458	-5,65339	316	1,394982
22,35827	5,02363	-3,80434	216	0,953532
22,18537	6,78422	-2,04375	116	0,512082
22,24124	7,68481	-1,14316	66	0,291357
22,09018	8,57118	-0,25679	16	0,070632

A. 2 Thrust

The calibration curve for the thrust is given by:

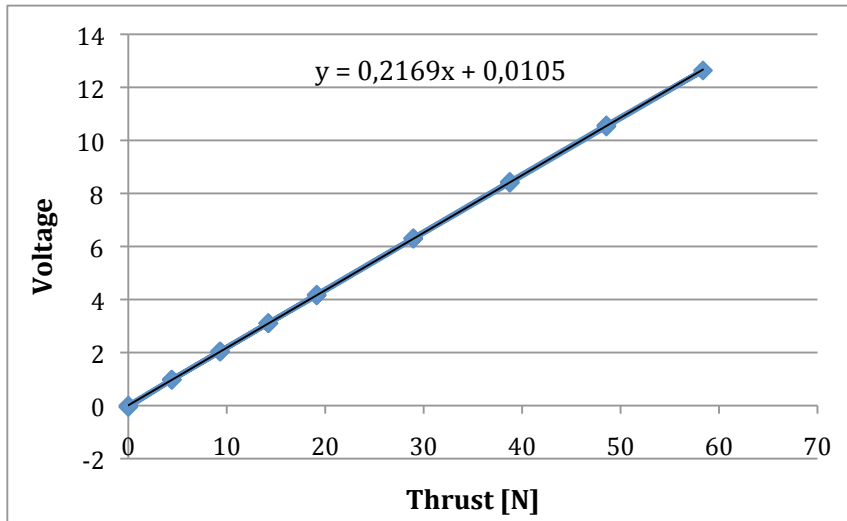


Figure A. 2 – Calibration curve, thrust.

From the calibration curve, the thrust is given by:

$$T = \frac{dE_{-Thrust}}{0.2169} \quad [N] \quad (A.2)$$

The off-set voltage was -8.542 V with an amplifier gain of 8. The data used to plot the calibration curve are shown in table A.2 below.

Table A. 2 – Calibration data, thrust.

Temp [C°]	E_Thrust [V]	dE_Thrust [V]	Mass (g)	Thrust (N)
23,9	-8,542	0,000	0	0,00
23,8	-7,565	0,978	450	4,41
23,7	-6,500	2,042	950	9,32
23,7	-5,432	3,110	1450	14,22
23,7	-4,362	4,181	1950	19,13
23,7	-2,231	6,312	2950	28,94
23,7	-0,103	8,439	3950	38,75
23,7	2,025	10,567	4950	48,56
23,7	4,095	12,637	5950	58,37
23,7	1,979	10,521	4950	48,56
23,7	-0,144	8,398	3950	38,75
23,7	-2,251	6,291	2950	28,94
23,7	-4,388	4,154	1950	19,13
23,7	-5,437	3,105	1450	14,22
23,6	-6,506	2,036	950	9,32
23,7	-7,565	0,977	450	4,41
23,6	-8,595	-0,053	0	0,00

A. 3 Pressure transducers

The contraction and the pitot tube used for wake measurements were each connected to a pressure transducer, manometer and amplifier. The pressure transducers were calibrated,

obtaining constants for the contraction and the pitot-static tube, both in unit $\left[\frac{Pa}{V} \right]$.

For all manometers, the slope scale used was 1:5.

A. 3. 1 Pitot-static tube

The pitot-static tube used measuring the horizontal velocity profiles was connected to a pressure transducer, which was again connected to a manometer used for the calibration. The amplifier gain was set to 5.

The calibration curve for the pressure transducer connected to the pitot probe is given in figure A.3, and the data used for plotting is given in table A.3.

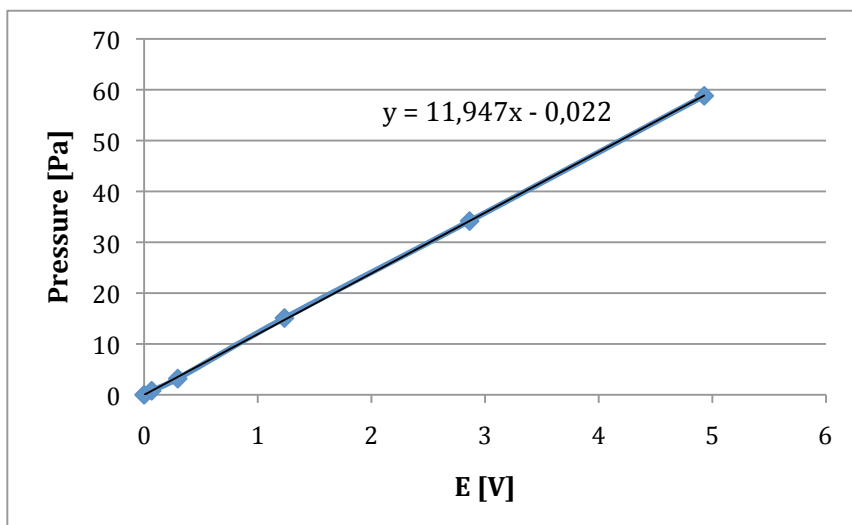


Figure A. 3 – Calibration curve, pitot-static tube.

Table A. 3 – Calibration data, pitot-static tube.

Temp [C°]	E_Pitot[V]	dE_Pitot[V]	h_MetSp[m]	P_dyn [Pa]
18	-8,56924	0	0	0
18,2	-8,50308	0,06616	0,0001	0,79461
18,2	-8,27346	0,29578	0,0004	3,17844
18,4	-7,33446	1,23478	0,0019	15,09759
18,5	-5,70541	2,86383	0,0043	34,16823
18,8	-3,64068	4,92856	0,0074	58,80114

A. 3. 2 *Contraction*

The contraction region used to find the velocity at the tunnel inlet was connected to a pressure transducer, and was also connected to a manometer used for the calibration. The manometer used together with the contraction was a newer type. The scaling on the methylated spirit column was given directly in Pascal, hence it was not necessary to calculate from mm to Pascal with this new manometer. The amplifier gain was set to 5.

The calibration curve for the contraction region and the data collected is given in figure A.4 and table A.4, respectively.

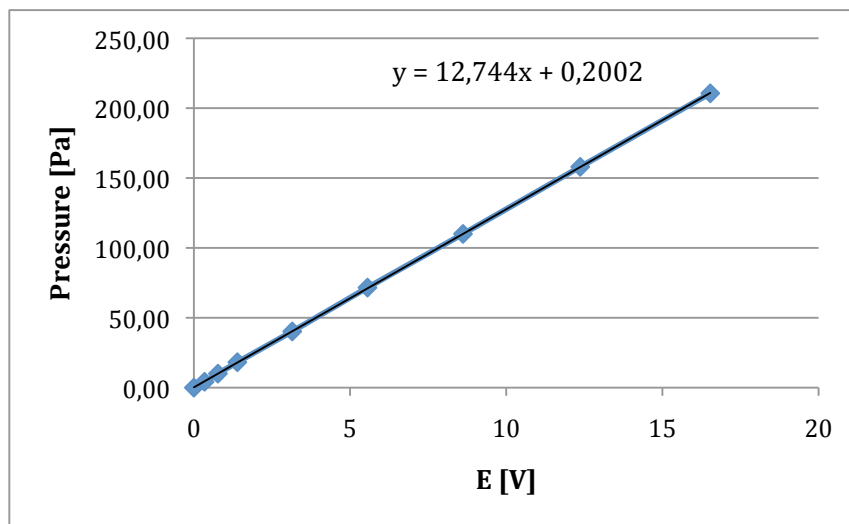


Figure A. 4 – Calibration curve, contraction.

Table A. 4 – Calibration data, contraction.

Temp [C°]	Tunnel RPM [Rev/min]	E_Contr [V]	dE_Contr[V]	P_dyn [Pa]
22,28867	0	-9,63918	0	0
22,27359	100	-9,29731	0,34187	4,2
22,2988	150	-8,86965	0,76953	10
22,38175	200	-8,2481	1,39108	18,2
22,59713	300	-6,49023	3,14895	40,2
23,03998	400	-4,08113	5,55805	71,6
23,78271	500	-1,02231	8,61687	110
24,7602	600	2,72967	12,36885	158
26,21494	700	6,89418	16,53336	210,6

A. 4 Hot-wire anemometer

The experiments conducted in the wind tunnel using hot-wire anemometry was very comprehensive, and was not calibrated or calculated for manually, but rather converted using a programmed FORTRAN routine as described earlier. The amplifier gain was set to 40, the offset voltage was found as -0.937×40 , and the overheat constant for the wire was calculated to be 1.596.

For the pipe flow experiment, the hot-wire anemometer was calibrated and plotted manually. A polynomial fit of fourth degree was chosen for the pipe flow experiment, resulting in four calibration constants as shown in Figure A. 5, with corresponding data given in Table A. 5.

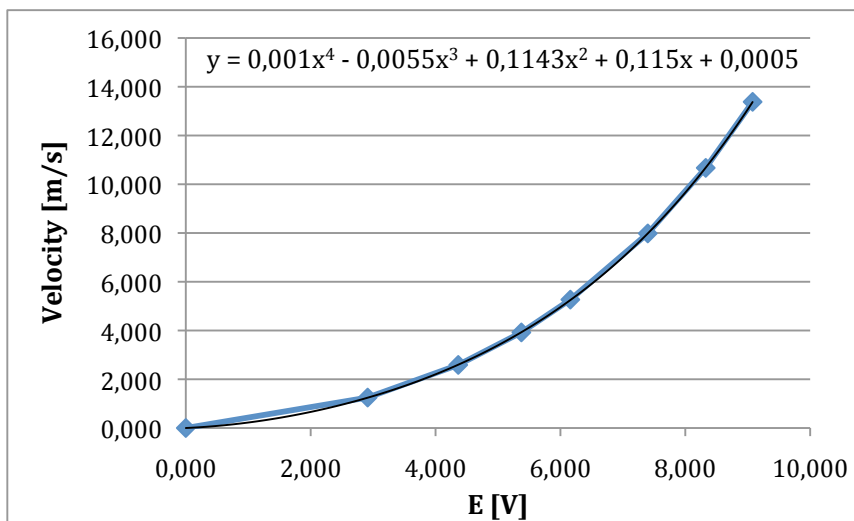


Figure A. 5 – Calibration curve, hot-wire anemometer.

Table A. 5 – Calibration data, hot-wire anemometer.

Temp[°C]	E_Pitot[V]	E_HW[V]	$\rho[\text{kg}/\text{m}^3]$	dE_Pitot[V]	dP [Pa]	V [m/s]	dE_HW[V]
15,51	-9,016	-9,351	1,191	0,000	0,000	0,000	0,000
15,49	-8,956	-6,438	1,191	0,060	0,929	1,249	2,912
15,51	-8,759	-4,987	1,191	0,257	3,988	2,588	4,364
15,58	-8,425	-3,976	1,191	0,591	9,157	3,922	5,375
15,63	-7,950	-3,192	1,190	1,066	16,513	5,267	6,159
15,77	-6,569	-1,952	1,190	2,447	37,903	7,982	7,399
16,06	-4,647	-1,023	1,189	4,369	67,674	10,671	8,327
16,56	-2,158	-0,273	1,187	6,858	106,215	13,380	9,078

APPENDIX B

B. 1

Horizontal mean velocity profiles at 3D downstream of the upstream turbine

